Australia's National
Science Agency

Visible-Near Infrared Spectral Library

Bobby Pejcic, Tina Shelton, Carsten Laukamp, Ian C. Lau, Monica LeGras
EP2022-5804
6.11.2022

National Virtual Core Library
AuScope

National Collaborative Research Infrastructure Strategy

Mineral Resources

Citation

Pejcic B, Shelton T, Laukamp C, Lau I C, LeGras M, (2022) Visible-near infrared spectral library, CSIRO, Australia, EP2022-5804, 1-62.

Copyright

Important disclaimer

Contents

Figures

Tables

Acknowledgments

This work was supported by AuScope Pty Ltd and the National Virtual Core Library (NVCL) project and CSIRO Mineral Resources. We gratefully acknowledge Tenten Pinchand for assistance with sample preparation and the ASD measurements. CSIRO researchers in the Discovery Program (Dr Heta Lampinen and Dr Andrew Rodger) are thanked for internally reviewing and providing important comments that improved the report.

Executive summary

Reflectance spectra collected of rocks and sediments in the visible to near infrared (VNIR) wavelength range (350 to 2500 nm) of the electromagnetic spectrum provide a unique fingerprint of a wide range of rock forming, alteration and ore minerals. Although the VNIR has been extensively used in a range of applications (i.e., environmental science, agricultural science, mineral exploration/mining, etc), the wavelength range between 350 to 2500 nm contains a great deal of spectral information that is difficult to understand. This is mainly due to the reflectance spectra not only depending on the chemical composition of the sample, but also many other factors contribute to the reflectance response such as the physical properties of the material (i.e., refractive index, surface roughness, particle size, etc) and the type of material (i.e., film/surface coating, moisture/water content).

This report describes CSIRO's new VNIR spectral reference library (VNIR SRL 2.0), which is planned to replace the VNIR SRL built into TSG in due course. The VNIR SRL 2.0 comprises reflectance spectra of 279 mineral samples over the 350 to 1350 nm wavelength range, which were acquired from single crystals, crystal aggregates, sand, pulp and rocks. It is important to note that the short-wave infrared (SWIR) region between 1300-2500 nm was also collected and is only provided for comparison purposes rather than detailed spectral peak assignment/analysis. Initially, VNIR and SWIR reflectance spectra were collected on about 2000 samples, and these were assessed for spectral features pertaining to the respective minerals of interest along with impurities related to associated minerals and other contaminants. If available, independent validation data (e.g. X-ray diffraction, scanning electron microscopy, inductively coupled plasma spectrometry and Fourier transform infrared spectroscopy) were used to evaluate the purity of the reference sample candidates. It is important to note that spectral validation of the 279 mineral samples which are contained in this report is an ongoing process and is work that is still being undertaken. The resulting VNIR SRL 2.0 collection comprises representatives from the following mineral groups: sulfides, oxides, hydroxides, carbonates, sulfates, phosphates, molybdates/tungstates, neosilicates, cyclosilicates, inosilicates and phyllosilicates.

1 Introduction

A large range of minerals exhibit characteristic spectral signatures in the visible and near infrared wavelength region (VNIR) of the electromagnetic spectrum (i.e., 350 to 2500 nm). For example, the VNIR has successfully been used to estimate the relative abundance of iron oxides and for discrimination of different iron oxyhydroxy species (e.g. Cudahy & Ramanaidou, 1997; Haest et al., 2011; Ramanaidou et al., 2015). Many transition metals, such as V, Cr, Mn, Fe, Ni and Cu produce strong absorptions in the VNIR (Burns, 1997), creating opportunities for rapid mineral characterisation supporting geoscience research, mineral exploration and ore body characterisation by means of hyperspectral VNIR sensors. In addition to transition metals, many rare earth elements (REEs) are VNIR-active, allowing cost-effective identification and determination of REEs and their host minerals by means of reflectance spectroscopy.

The Spectral Geologist (TSG^{TM}) software features a VNIR spectral reference library (SRL), which underlies the automated mineral matching of a suite of VNIR-active minerals and other materials performed by The Spectral Assistant (TSA) (Berman et al., 2017). However, the provenance and composition of mineral groups and species present in the VNIR-SRL built into TSG version 8.1.0.4 is largely imprecise. In addition, the VNIR-SRL is incomplete and not fully representative of the mineral groups and species found across Australia (Laukamp et al., 2016). The collection of iron oxides and sulphides are inadequate and other increasingly important mineral species, such as the REE-bearing carbonates and phosphates, are completely missing. The previous VNIR-SRL consists of 17 minerals from 450nm to 1100 nm. The spectra of the minerals are averages of a number of (mostly ASD) spectra for each mineral. It should be noted that, with the exception of the REE-bearing minerals, the spectral reflectance characteristics of most materials in the VNIR form relatively low-frequency, smooth curves, somewhat different to the sharper vibrational features observed in the SWIR. This is important to appreciate as spectral matching and fitting algorithms generally work less effectively and generate greater ambiguity than, say, modelling spectral mixtures in the SWIR. It is for this reason that many of the VNIR minerals are by default "turned off" in TSA's unmixing library (TSG version 8.1.0.4) and are only available by explicitly turning them back on again.

This report describes a new set of minerals that form part of CSIRO's VNIR SRL 2.0, which comprises now a larger suite of iron oxides, sulphides, sulphates, REE-bearing phosphates and carbonates as well as silicates. VNIR and SWIR reflectance spectra of about 2000 mineral samples that potentially included the minerals targeted for the VNIR SRL 2.0, were evaluated for their spectral purity across the 350 to 2500 nm wavelength range. Sample types included single crystals, crystal aggregates, pulps, sand, and rocks. A sample was included in the VNIR SRL 2.0, when deemed sufficiently pure (>70%) according to previous XRD analysis, comparison of spectra to literature and/or when no alternative candidates of the respective mineral species were available. Where possible, validated samples that are part of the previous SRLs that were developed by CSIRO and in the frame of the National Virtual Core Library (NVCL) project, were drawn from. The VNIR SRL 2.0 comprises the 350 to 1350 nm wavelength range. The VNIR measurement setup and data processing are described in chapter 3 ("Methods"). VNIR spectra and a brief description of major absorption features can be found in chapter 4 ("Mineral groups and species"). A summary of VNIR-functional groups and scripts

designed to extract the relative intensity and wavelength positions of REE-related absorption features is provided in chapter 5.

It should be noted that the collection presented in this report is not comprehensive in that it does not represent the full variability of VNIR spectral signatures of all relevant rock forming and key alteration minerals. It is thus a work in progress. Chapter 6 provides a summary of the VNIR SRL 2.0 as well as recommendations with regards to 1) additionally required validation of already included reference samples, 2) additional reference material required, and 3) preparations required for routine processing of VNIR reflectance spectra in TSG.

2 Source of datasets and validation

Reference samples for the VNIR SRL 2.0 were sourced from a variety of collections, including CSIRO's NVCL, Mitchell and BHP collections. Many of the reference samples are also part of CSIRO's thermal infrared (TIR) SRL (version MS9) and CSIRO's mid-infrared (MIR) SRL (version 0.1) and/or were investigated in the frame of the NVCL Spectral Reference Library activity over recent years (LeGras et al., 2018, 2019; LeGras and Lau, 2019; LeGras and Laukamp, 2019; Pejcic et al., 2021; Schodlok et al., 2016a). Table 1 provides a summary of the various collection and related references, as well as the respective targeted mineral groups and number of samples of each mineral group used for VNIR SRL 2.0. A detailed list providing information about the type, locality, available additional analytical results and references for each of the 279 reference samples can be found in Appendix A. An overview list of the mineral groups and species contained in VNIR SRL 2.0, organised according to the Dana classification scheme, can be found in Appendix B. A brief overview of the source datasets and validation methods is provided further down in this section. This overview focusses on the geological setting and mineralogical characteristics of the respective case studies. Technical details can be found in the referenced publications.

Table 1 Collections and related references, targeted mineral groups and number of samples of each mineral group used for VNIR SRL 2.0

Reference/collection	(main) mineral groups	No. of samples
CSIRO TIR SRL (Schodlok et al., 2016a)	Carbonates, epidote	7
(LeGras et al., 2018) EP183095	Micas	3
(LeGras and Laukamp, 2019) EP184276	Pyroxenes, pyroxenoids	9
unpublished, NVCL collection & donations	Various	20
unpublished, Mitchell collection	Various	208
unpublished, BHP mineral collection	Various	2
Unpublished, WA Museum	Various	30
	Total	*279*

2.1 Validation

Reference sample candidates for the VNIR SRL 2.0 were selected based on the following: 1) whether distinct absorption features could be expected from those mineral groups and species; and 2) whether the respective mineral groups and species are of high interest for the mineral resources sector – hence the wide range of sulphides, iron oxides and REE-bearing minerals.

Where available existing published and recently collected analytical results of the reference samples were included in this report and results are listed in Appendix A. Independent analytical techniques include:

- X-ray diffraction; XRD (21 samples): (LeGras et al., 2018, 2019; LeGras and Laukamp, 2019; Pejcic et al., 2021; Schodlok et al., 2016a) + unpublished NVCL and Mitchell collection results
- Inductively coupled plasma (ICP) spectrometry (44 samples)
- Scanning electron microscopy; SEM (7 samples): (LeGras and Laukamp, 2019)
- Electron probe microanalysis; EPMA (3 samples): (LeGras et al., 2018)
- X-ray fluorescence; XRF (3 samples): (Schodlok et al., 2016a)

Where XRD results are available, the reference samples were classified according to the following three categories (column S in "VNIR_SRL_report_AppendixA.xlsx"):

- "Pure (GT[1]90 XRD)": target mineral species amounts to +90% according to XRD
- "80% pure (90to80)": target mineral species amounts to 80 to 90% according to XRD
- "Impure (LT80)": target mineral species amounts to less than 80% according to XRD.

An additional fourth category to be determined "tbd" is reserved for all remaining reference samples, in which case XRD results were not yet available at the publication date of this report.

It should be noted that differences in sampling area and/or sampling volume may exist when comparing XRD and reflectance spectroscopic analysis, depending on the sample type. In the case of a given powder sample, it can be assumed that the sample material is homogeneous, and the acquired diffractometer and spectrometer patterns are representative for the same mineral assemblage. However, if samples were crushed to a finer fraction for XRD after the acquisition of reflectance spectra, the differences in grain size will have a significant impact, especially on the reflectance intensity. In the case of rock samples and crystal aggregates, care was taken that material from XRD was acquired from the same sample material of the targeted mineral species.

All reference sample material are natural samples and were available in one or more of five forms (column "sample type" in Appendix A):

- Single crystals: this includes crystals of various size, typically between 0.5 and 5 cm in length. Some single crystals contain visual impurities, in which case VNIR-SWIR reflectance spectra were collected from the mostly pure side of the crystal.
- Crystal aggregates: this includes aggregates of smaller crystals, typically between 0.05 and 0.5 cm in diameter, that are orientated in different ways to each other (e.g. randomly or radially). Crystal aggregates can include visibly small amounts of impurities.
- Rock samples: these include all samples, where the target mineral is present in a mixed mineral assemblage and finely intergrown with other minerals, mostly at microscopic scale.

[1] GT - greater than, LT – less than.

- Pulp samples: biotite MES001 and goethite M0765.

2.2 TIR SRL

The thermal infrared (TIR) spectral reference library (SRL) is a collection of replicate hyperspectral reflectance measurements made on TIR-active rocks and minerals with a HyLogger-3 instrument. The samples for this library were acquired from a variety of sources. It is an important component of interpreting reflectance spectra acquired with TIR-capable hyperspectral drill core scanners, such as the HyLogger-3 and HyLogger-4 systems being utilised at the NVCL nodes located at six Australian State and Territory Geological Surveys (Schodlok et al., 2016b). The TIR SRL was designed to be used by the TIR component of TSA algorithm (Berman et al., 2017) in the TSG software package. Mineral unmixing algorithms, such as TSA, and other matching algorithms are highly reliant on: 1) on accurate assignment and purity of the reference samples (keyword: validation); and 2) on a comprehensive SRL, where mineral species that occur in the respective dataset are represented (keyword: comprehensive). The validation process of the TIR SRL has been ongoing (Laukamp et al., 2015a) and independent validation results, for example by means of QXRD, SEM- energy-dispersive X-ray spectroscopy (EDS) or EPMA that were collected for improving the TIR SRL sample collection were available for the VNIR SRL 2.0 (Table 2). Whole rock geochemistry (XRF) is available for three of the TIR SRL samples (Table 3).

Table 2 TIR SRL samples used in VNIR SRL 2.0 listing XRD results of major components (in wt%). Samples with companion XRF measurements shown in Table 3 are marked with an asterisk.

Sample name	Main mineral species of interest	Main mineral group of interest	Pure (GT90 XRD) / 80% pure (90to80) / Impure (LT80) / tbd	iron oxides and spinels tot	carbonate group tot	sulphate group tot	epidote	schorl	mica group tot	talc	chlorite group tot	quartz tot	feldspar tot
M0312*	aragonite	carbonate	pure	0	100	0	0	0	0	0	0	0	0
M0898	strontianite	carbonate	pure	0	100	0	0	0	0	0	0	0	0
NR-MAG-04	magnesite	carbonate	80% pure	0	80	0	0	0	0	0	0	2	0
NR-WIT01b	witherite	carbonate	80% pure	0	80	0	0	0	0	0	0	0	0
M2098*	siderite	carbonate	80% pure	2	80	0	0	2	0	0	0	2	0
NR203*	dolomite	carbonate	pure	0	90	0	0	0	0	0	0	0	0
MCU-EPI-1	epidote	epidote gro	80% pure	0	0	0	80	0	2	0	0	15	0

Table 3 Whole rock geochemistry (XRF) available for TIR SRL samples used in VNIR SRL 2.0 (Schodlok et al., 2016a)

Sample name	SiO2 [%] (XRF)	TiO2 [%] (XRF)	Fe2O3 [%] (XRF)	MnO [%] (XRF)	MgO [%] (XRF)	CaO [%] (XRF)	P2O5 [%] (XRF)	H2O [%] (XRF*)	CO2 [%] (XRF*)	Sum [%] (XRF)	Ba [ppm] (XRF)	Rb [ppm] (XRF)	Sr [ppm] (XRF)	Zn [ppm] (XRF)	Zr [ppm] (XRF)
M0312	<0.01	0.01	0.01	0.011	0.19	54.88	0.086	0.385	43.665	99.237	335	<10	10829	<10	303
M2098	1.86	0.011	55.1	2.32	3.08	0.61	0.01	0.715	36.675	100.381	39	56	<10	606	16
NR203	<0.01	0.011	0.13	0.014	21.56	31.12	0.011	0.16	47.87	100.876	50	60	138	14	<10

2.3 Dark Mica

A large range of dark micas were analysed by means of XRD and EPMA during previous work of the NVCL Spectral Reference Library activity (LeGras et al., 2018). Three of these samples are included in the VNIR SRL 2.0. All three samples are pure micas according to the XRD results (Table 4). Fluorine content, which can have an impact on the strength of hydroxyl-related absorptions, ranges from 0.33 to 4.13 % (sample M1593). The Tschermak exchange values ([Al+Si]/[Al+Si+Fe+Mg]) range from 0.56 to 0.61 (Table 4).

Table 4 Dark mica reference samples used in VNIR SRL 2.0, listing their classification according to XRD as well as EPMA-derived geochemistry. The Tschermak exchange values ([Al+Si]/[Al+Si+Fe+Mg]) calculated from EPMA results are listed in the last column from left. Detailed XRD results can be found in Appendix A.

Sample name	Main mineral species of interest	Main mineral group (MIR SRL classification)	Pure (GT90 XRD) / 80% pure (90to80)	EPMA																Tschermaks
				F	Cl	Ca	Rb	Si	Mg	Al	Mn	Na	Ti	K	Ba	Cr	Fe	Ni	O	
M1593	biotite	biotite subgroup ("dark mica")	pure	4.13	0.23	0	1.34	16.04	0.96	9.91	0.43	0.13	0.42	7.65	0.03	0.01	19.59	0	35.49	0.56
MES014	phlogopite		pure	0.33	0	0.02	0.35	17.81	15.05	8.43	0.13	0.13	0.01	8.53	0.32	0.01	1.84	0	40.15	0.61
M1589	phlogopite		pure	5.3	0.01	0	0.25	17.91	12.38	7.31	0.07	0.04	1.86	8.51	1.04	0.02	5.69	0.01	39.86	0.58

2.4 Pyroxene and pyroxenoid

A large range of pyroxenes and pyroxenoids were analysed by XRD and SEM as part of previous work on the NVCL Spectral Reference Library activity (LeGras and Laukamp, 2019). Nine of these samples have been included in the VNIR SRL 2.0 (Table 5). According to XRD, three of the nine samples are pure pyroxene or pyroxenoid, four are 80% pure and two are impure. Whereas the pyroxenoids are largely pure mineral samples, most of the pyroxenes are mainly associated with amphiboles and feldspars. According to major element chemistry by means of SEM-EDS (Table 6), pyroxenes that were classified as augite (LeGras and Laukamp, 2019) are characterised by varying Mg/Fe-ratios. The diopside sample 196 is slightly enriched in Fe, but otherwise is of typical diopside composition. The enstatite MES 041 is enriched in Fe (4.13 wt%), but very low in Ca and Al. Hedenbergite sample NR139 shows the characteristic Fe-rich composition, whereas as sample NR162 shows an unusually high Mg-content.

Table 5 Pyroxene and pyroxenoid reference samples used in VNIR SRL 2.0, listing their classification according to XRD of sample pulps as well as SEM-derived geochemistry of target minerals in wt % and normalised to 100 (LeGras and Laukamp, 2019). Minerals other than pyroxene and pyroxenoid are abbreviated: act – actinolite, chl – chlorite, ms – muscovite, PbS – galena, qtz – quartz.

Sample name	Main mineral species of interest	Main mineral group of interest	Mineral	Pure (GT90 XRD) / 80% pure (90to80) / Impure (LT80) / tbd	Impurities (based on XRD) (based on chemistry)	SEM									
						O	Si	Ca	Na	Fe	Mg	Al	Mn	Cr	Total
MES085	aegirine	pyroxene	aegirine + orthoclase	impure	37	41.98	28.17	0.32	7.87	20.22	0.09	1.3	0.05	0	100
m1865	augite	pyroxene	augite + act +qtz	80% pure	11	44	26.75	14.14	1.15	5.2	7.69	1	0	0.08	100.01
m2222	augite	pyroxene	augite + qtz + act	80% pure	11	42.43	25.73	14.06	0.89	10.82	4.21	1.28	0.49	0.09	100
196	diopside	pyroxene	diopside + ms + act	80% pure	13	45	27.07	13.99	0.65	1.28	11.32	0.48	0	0.2	99.99
mes041	enstatite	pyroxene	enstatite (+ talc)	pure	3	45.86	25.01	0.29	0.76	4.13	23.23	0.47	0.15	0.11	100.01
NR139	hedenbergite	pyroxene	hedenbergite + qtz + chl + PbS	impure	33	40.6	24.56	14.66	0	14.59	0.27	1.41	3.84	0.07	100
NR162	hedenbergite	pyroxene	hedenbergite	pure	0	43.96	25.19	15.71	0.71	2.23	11.01	0.75	0.11	0.34	100.01
MES183	rhodonite	pyroxenoid	rhodonite	pure	0	NULL	NULL	NULL	NULL	NULL	NULL	NULL	NULL	NULL	NULL
m1094	rhodonite	pyroxenoid	rhodonite + PbS	80% pure	12	NULL	NULL	NULL	NULL	NULL	NULL	NULL	NULL	NULL	NULL

Table 6 Major element ratios of pyroxenes based on SEM (LeGras and Laukamp, 2019).

Sample name	Main mineral species of interest	Ca/ (Ca+Mg+Fe+Al)	Mg/ (Ca+Mg+Fe+Al)	Fe/ (Ca+Mg+Fe+Al)	Al/ (Ca+Mg+Fe+Al)
MES085	aegirine	0.01	0.00	0.92	0.06
m1865	augite	0.50	0.27	0.19	0.04
m2222	augite	0.46	0.14	0.36	0.04
196	diopside	0.52	0.42	0.05	0.02
mes041	enstatite	0.01	0.83	0.15	0.02
NR139	hedenbergite	0.47	0.01	0.47	0.05
NR162	hedenbergite	0.53	0.37	0.08	0.03

2.5 Mitchell, BHP & NVCL collections

About 2000 VNIR-SWIR reflectance spectra were evaluated for their spectral purity across the 350 to 2500 nm wavelength range. However, the focus was on the wavelength range 350 to 1350 nm and spectra were included in VNIR SRL 2.0 when deemed sufficiently pure and/or when no alternative candidates of the respective mineral species were available.

2.6 WA Museum collection

Thirty-one samples were borrowed from the WA Museum collection, mainly comprising phosphates and REE-bearing minerals. These samples are labelled as “unpublished, WA Museum collection” in column I (Reference) of Appendix A. However, these samples have not yet been validated and further work is needed to establish their purity and suitability.

3 Methods

3.1 Data acquisition

All reflectance spectroscopy measurements were performed at CSIRO (ARRC, Kensington) using an ASD FieldSpec3 spectrometer (Analytical Spectral Devices, model A122300) over the wavelength range 350 to 2500 nm (see Figure 1). The ASD spectrometer was controlled and operated using RS^3 software. A white reference standard (Spectralon) was used to optimise and calibrate the spectrometer. A white reference was collected every ten minutes. The spectrometer was warmed up for at least 30 minutes prior to commencing the measurements. A Mylar reference was also employed to check the performance of the instrument. Reflectance spectra were collected using at least 20 scans at a sampling interval of 1.4 nm for the region between 350-1000 nm and 2 nm for the 1000-2500 nm range, both regions resampled to 1 nm. A 512 element silicon photodiode array detector was used for the 350-1000 nm region and InGaAs photodiodes for the 1000-2500 nm region. Two different probes (contact or muglight) were used depending on if the sample was a powder or a rock. All measurements were made in duplicates.

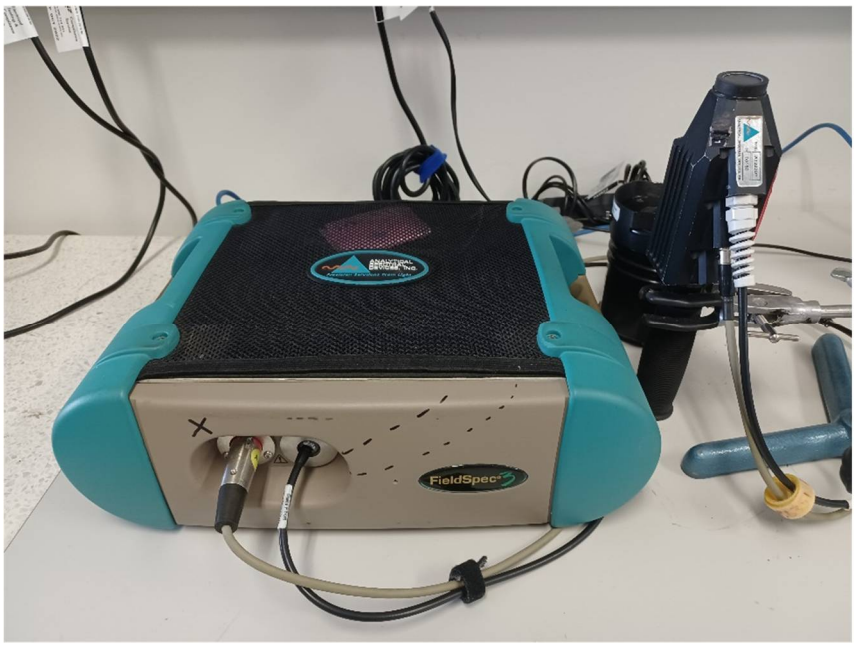

Figure 1 Photograph of the instrument and experimental setup used.

3.2 Data processing – pre-processing

The processing of VNIR-SWIR reflectance spectra was performed using TSG software version 8.0.7.4. The spectra were corrected to absolute reflectance and the peak/through features were determined.

3.3 ICP spectrometry

Validation studies using inductively coupled plasma (ICP) spectrometry were undertaken on selected mineral and rock samples. ICP analysis was performed by LabWest Pty Ltd (Perth, Western Australia) using optical emission spectrometry (ICP-OES: Perkin Elmer Optima 7300DV) and mass spectrometry (ICP-MS: Perkin Elmer Nexion 300Q). Various methods were used (alkaline fusion and multi-acid) to digest the samples prior to measurement. Multi-element analysis (MMA technique) is a microwave-assisted, HF-based digestion that effectively offers total recovery for all but the most refractory of minerals. A portion of the sample was digested in an HF-based acid mixture under high pressure and temperature in microwave apparatus followed by the determination of 64 elements including rare earths. Whole rock analysis (AF method) was also performed by fusing the samples in an alkaline salt (sodium peroxide) followed by dissolution in nitric acid. All rock samples were crushed and pulverised to less than 50 microns using a ball mill.

4 Mineral groups and species

Mineral groups and species present in the VNIR SRL version 2.0 are listed in Table 7. The full list of mineral species contained within VNIR SRL version 2.0 is presented in Appendix B (included spreadsheet VNIR_SRL_report_AppendixB.xlsx). Many samples exist covering the following mineral groups: carbonates, iron oxides and phosphates and sulphides. However, the amount of single mineral species within a respective mineral group can vary greatly (Table 7).

In this chapter, reflectance spectra of the respective mineral groups are shown in the full wavelength range that was collected using an ASD FieldSpec3 (350 to 2,500 nm). However, for many reference samples, MIR and TIR reflectance spectra are available as well (listed in Appendix A). The major VNIR absorption features are described briefly and some are described in more detail in chapter 5. The spectral behaviour within VNIR wavelength range is predominantly controlled by the electronic modes, which involve the transfer of electrons from lower to higher energy states within electron orbits (CFA – crystal field absorption) or from ligand to the cation (CTS – charge transfer). For detailed description of features in spectra related to electronic modes in rock forming minerals the reader is referred to (Burns, 1993).

Table 7 Mineral groups contained within the VNIR SRL 2.0 and number of samples that contain the respective mineral groups. The numbers in the mineral group column signify the Dana class. The number in the mineral species column signify the number of reference samples of each mineral species.

Mineral group (Dana class)	Mineral Subgroup (MIR SRL)	Mineral species (MIR SRL)	Number of samples
Native Elements (1)	Native elements	gold [1], copper [3], sulfur [2]	6
Sulfide Minerals (2)	Sulfide group	arsenopyrite [8], bornite [11], boulangerite [2], bournonite [2], chalcocite [13], chalcopyrite [15], cinnabar [2], cobaltite [1], covellite [3], galena [4], lollingite [1], marcasite [1], molybdenite [7], nickeline [2], proustite [1], pyrargyrite [1], pyrite [9], pyrrhotite [2], sphalerite [2], stannite [1], stibnite [13], stromeyerite [1], tennantite [1] tetrahedrite [2]	105
simple oxides (4)	Cuprite	cuprite [3]	3
	Rutile group	cassiterite [1]	1
	Iron oxides	hematite [7]	7
Hydroxides and Oxides with OH (6)		goethite [15], lepidochrocite [1]	16
multiple oxides (7)		magnetite [3]	3
Hydroxyhalides (10)	Atacamite group	atacamite [2]	2
Carbonate (14, 16)	Carbonate group	ankerite [1], aragonite [1], azurite [5], bastnasite [2], calcite [2], cerussite [1], dolomite [4], gaspeite [3], magnesite [1], malachite [5], parasite [1], pyroaurite [1], rhodochrosite [3], siderite [2], strontianite [2], synchysite [1], witherite [2]	37
Anhydrous Sulfates with OH or Halogen (30)	Sulfate group	jarosite [2]	2
Phosphates (38, 41)	Phosphate group	apatite [4], monazite [13], xenotime [3]	20

Anhydrous Molybdates and Wolframates (48)	Wolframite and scheelite series	wolframite [9], scheelite [2]	11
Nesosilicate (51, 52)	Phenakite & olivine	olivine unclassified [4], willemite [1]	5
	Garnet	almandine [2], andradite [2], calderite [1], grossular [1], pyralspite unclassified [2], pyrope [2], spessartine [1], uvarovite [3]	14
	Silicate apatite	britholite [2]	2
Sorosilicate (58)	Epidote	epidote unclassified [3]	3
Cyclosilicates (61, 64)	Tourmaline	tourmaline [5]	5
	Eudialyte group	eudialyte & mesodialyte [3]	3
Inosilicate (65, 66, 69)	Pyroxene	aegirine [1], augite [2], diopside [3], enstatite [3], hedenbergite [3], pyroxene unclassified [1]	13
	Pyroxenoid	rhodonite [3]	3
	Pyroxmangite group	pyroxmangite [1]	1
	Amphibole	actinolite [2]	2
	Other inosilicate	rhonite [1]	1
Phyllosilicate (71, 74)	Biotite subgroup ("dark mica")	biotite [4], phlogopite [2]	6
	Muscovite subgroup ("white mica")	fuchsite [1]	1
	Palygorskite-sepiolite group	falcondoite (garnierite) [2]	2
	Chrysocolla	chrysocolla [5]	5

4.1 Native elements

Reflectance measurements were made over the wavelength range 350 to 2500 nm on a number of different native elements and Figure 2 shows their VNIR-SWIR reflectance spectra. The sulfur samples displayed very low reflectance values below 420 nm, noting that the reflectance decreased sharply between 500 to 420 nm. In addition, weak trough features were evident at 1430 nm and 1925 nm. By contrast, the reflectance values for both the gold and copper samples gradually decreased between 600 to 350 nm. Subsequently, the SWIR wavelength range of these samples were unremarkable, and they did not display any significant features between 1000 to 1800 nm, apart from one of the gold samples (M0071) which seemed to have a very broad trough feature at ~1400 nm.

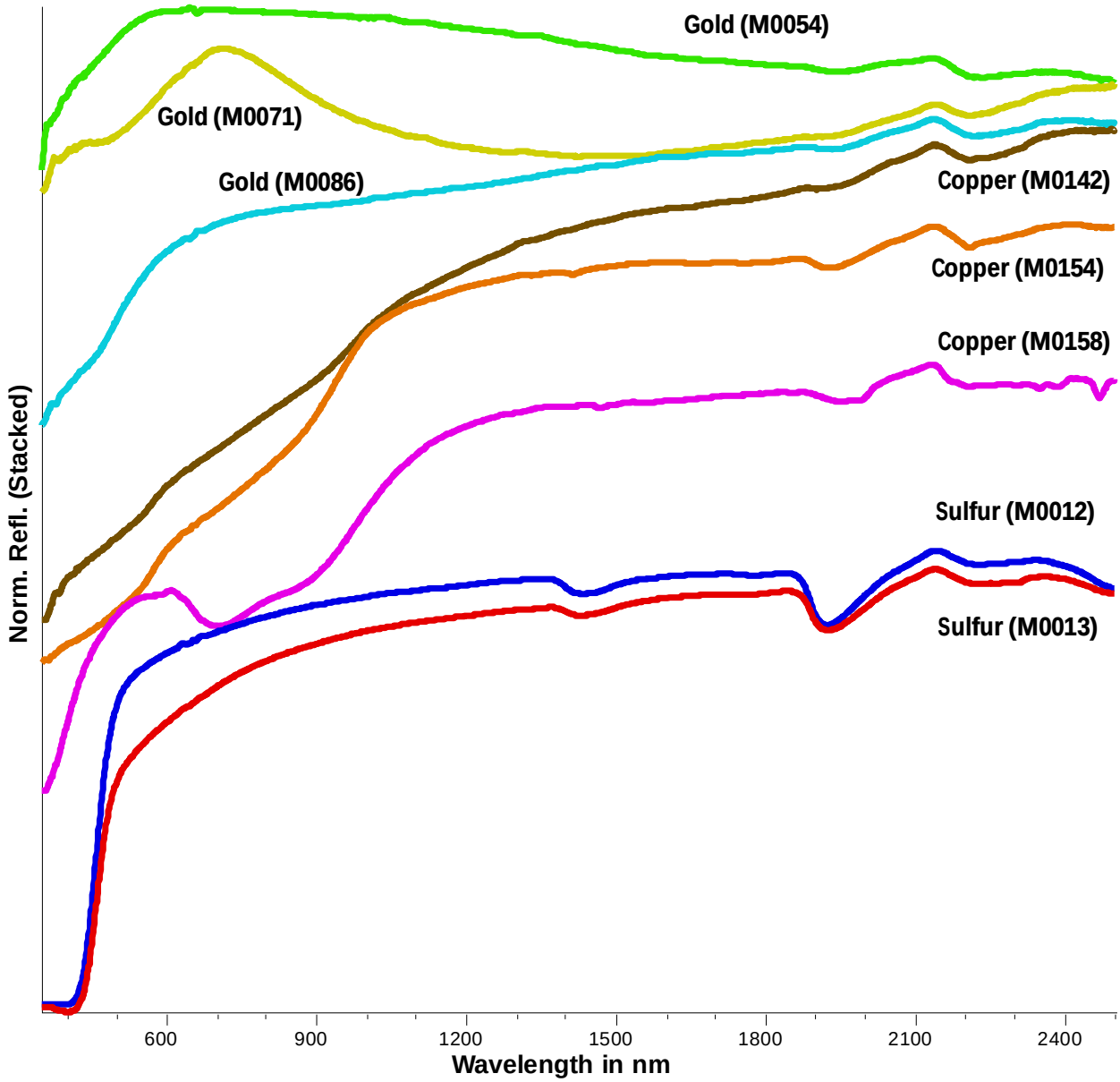

Figure 2 UV-VNIR-SWIR reflectance spectra (350 to 2500 nm) of gold, copper and sulfur.

4.2 Sulfide Minerals

The reflectance spectra of a range of different sulfide minerals were measured and Figure 3 shows the VNIR-SWIR reflectance spectra over the 350 to 2500 nm wavelength region. The pyrite samples displayed low reflectance values below 400 nm, noting that the reflectance gradually decreased between 700 to 350 nm. Generally, the SWIR wavelength range of the sulfides were unremarkable, and they did not display any significant features between 1400 to 2500 nm. In many cases (except for the covellite sample), the sulfide minerals displayed low reflectance values below 400 nm, noting that the reflectance generally decreased between 500 to 350 nm. The diffuse reflectance spectra and optical properties of a range of sulfides were discussed by (Wood and Strens, 1979). The wavelength position of sulfide reflectance minima and maxima in the UV and VNIR wavelength range depend on the composition and crystal structure of the respective sulfides. Plotting the wavelength position of the reflectance minima in the UV to VNIR wavelength range against the minimum in the 1st derivative of said wavelength range allows a grouping of different sulfide mineral species (Figure 4).

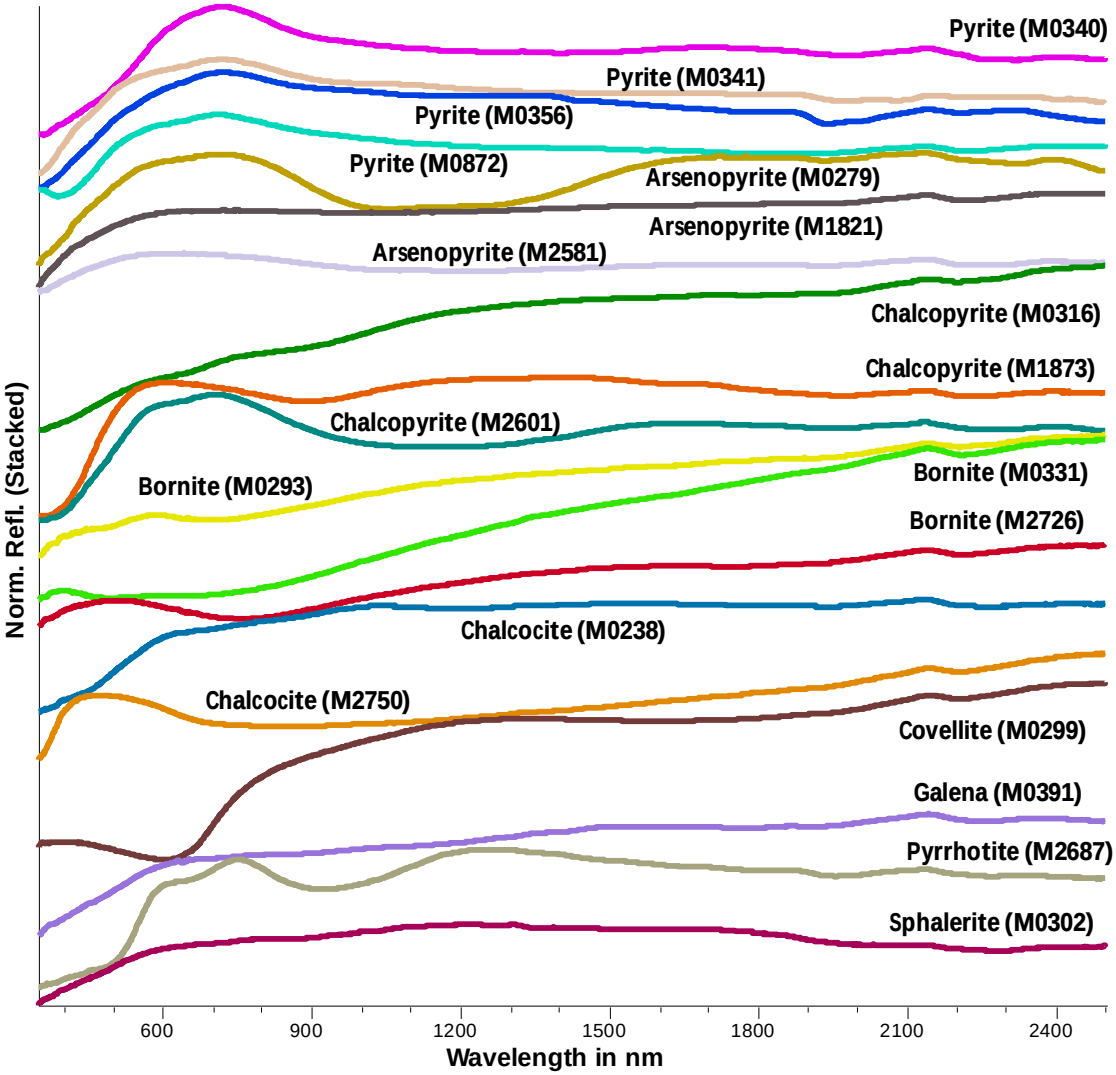

Figure 3 UV-VNIR-SWIR reflectance spectra (350 to 2500 nm) of sulfides.

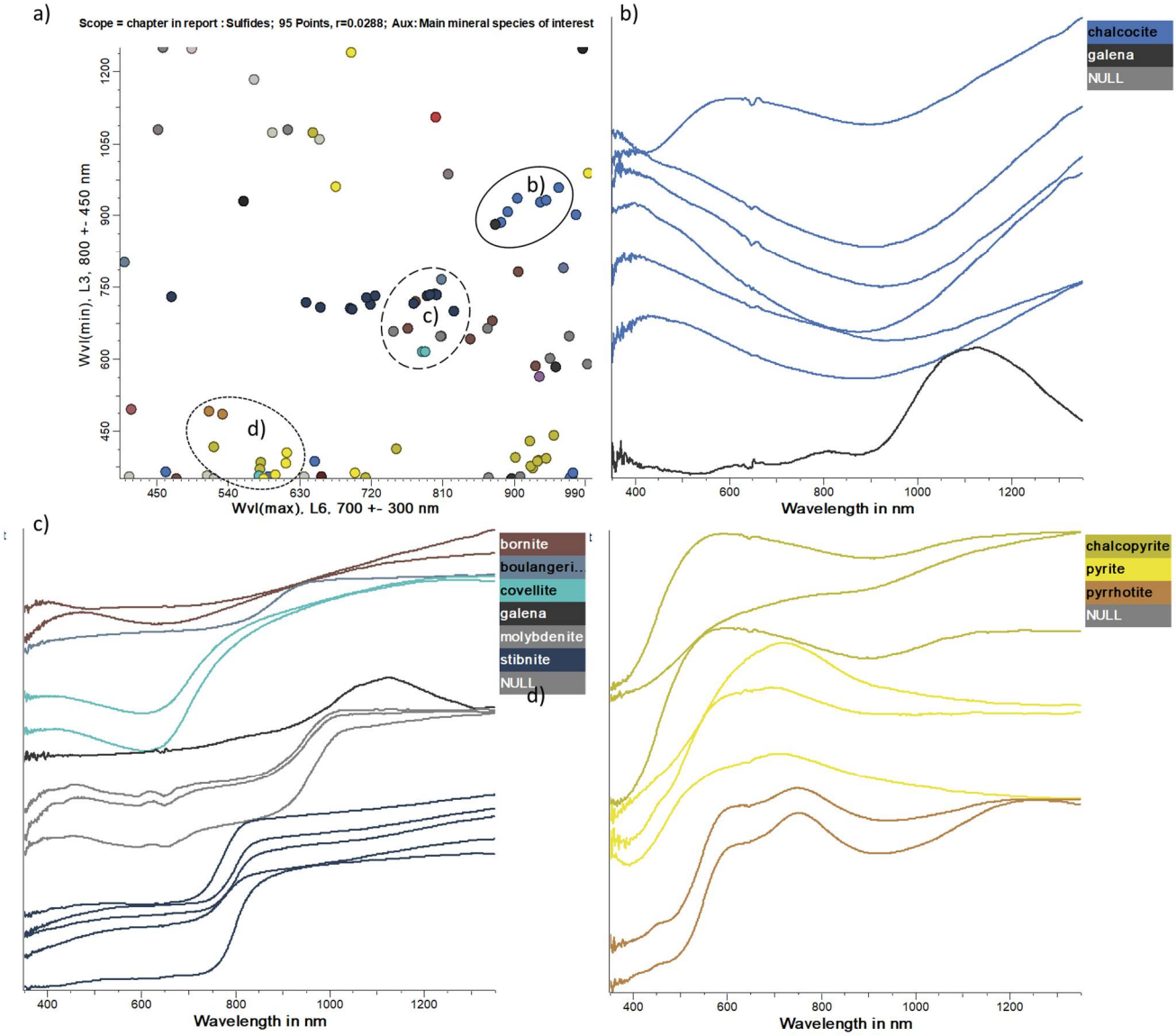

Figure 4 VNIR sulfide reflectance spectra: a) wavelength position of the maximum reflectance in the 400 to 1100 nm wavelength range (hull quotient applied) on the x-axis plotted against the wavelength position of the minimum in the 1st derivative of the 350 to 1250 nm wavelength range (local hull applied), coloured by mineral species; b), c) and d) normalised VNIR reflectance spectra of mineral species highlighted in three respective circles in a).

4.3 Simple oxides, hydroxides and oxides with OH, multiple oxides

The reflectance spectra of different iron oxide minerals were measured and Figure 5 shows the VNIR-SWIR spectra over the wavelength range 350 to 2500 nm. The hematite samples contained generally three trough features at 512, 652 and 885 nm. These bands were present in all hematite samples. The 885 nm feature was broad and the wavelength position varied slightly between the different hematite samples. The reflectance between 1200 to 2500 was relatively constant/similar and no major features (apart from a weak trough at 2207 nm) appeared in this region. Interestingly, all of the magnetite samples contained the trough at 2207 nm. In the case of magnetite, no

significant trough features were observed apart from a band at ~994 nm which was present on some of the samples. However, a weak trough was present around 468 nm and this was observed only on some samples.

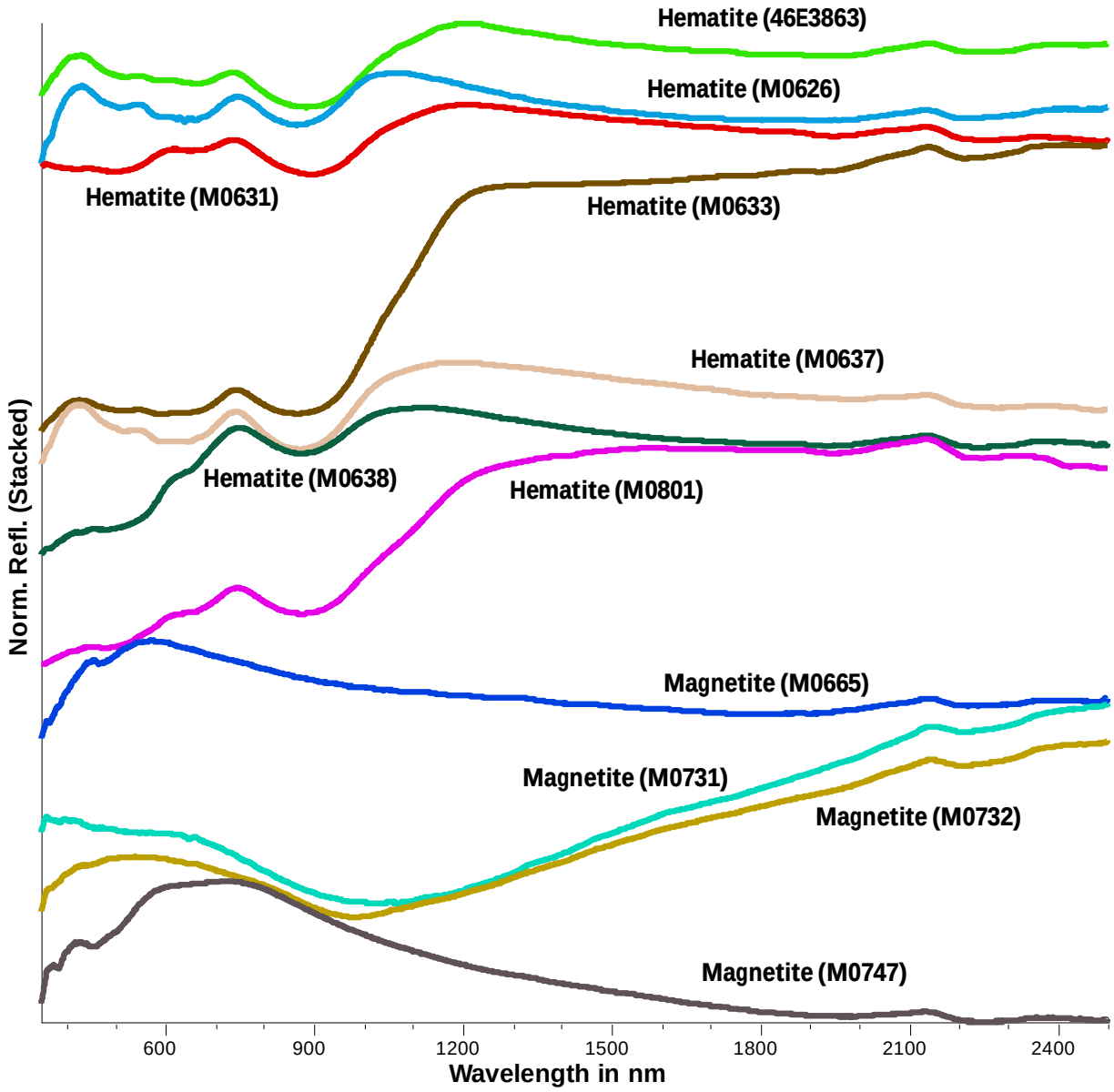

Figure 5 UV-VNIR-SWIR reflectance spectra (350 to 2500 nm) of selected iron oxide minerals.

Figure 6 shows the VNIR-SWIR spectra of different iron hydroxide minerals. The goethite samples contained generally trough features at 493 (weak), 665 (weak), 950 (broad), 1452, 1784 (weak) and 1940 nm. These bands were present on all samples. The 950 nm feature was broad and the wavelength position did not vary much between the different goethite samples. Interestingly, the lepidocrocite sample only contained a weak trough feature at 493 nm.

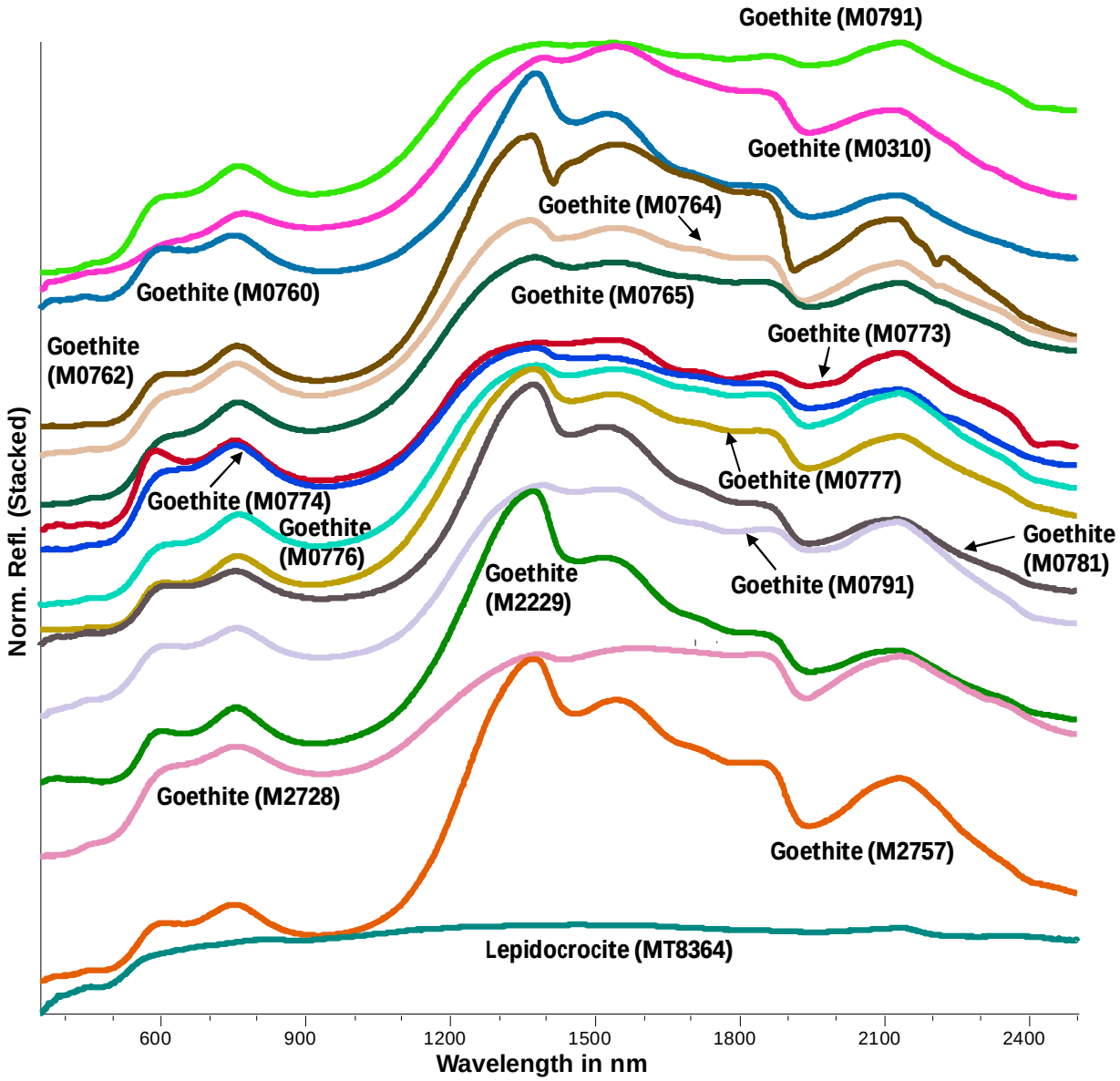

Figure 6 UV-VNIR-SWIR reflectance spectra (350 to 2500 nm) of selected hydroxide minerals.

The charge transfer absorption (CTA) of ferric iron at around 900 nm is the most prominent feature in VNIR reflectance spectra of iron oxides and its wavelength position can be used to discriminate hematite from goethite (Cudahy and Ramanaidou, 1997). In hematite samples of the VNIR SRL 2.0, the CTA is located between 880 and 900 nm, whereas the goethite samples range from 900 to 920 nm (Figure 7).

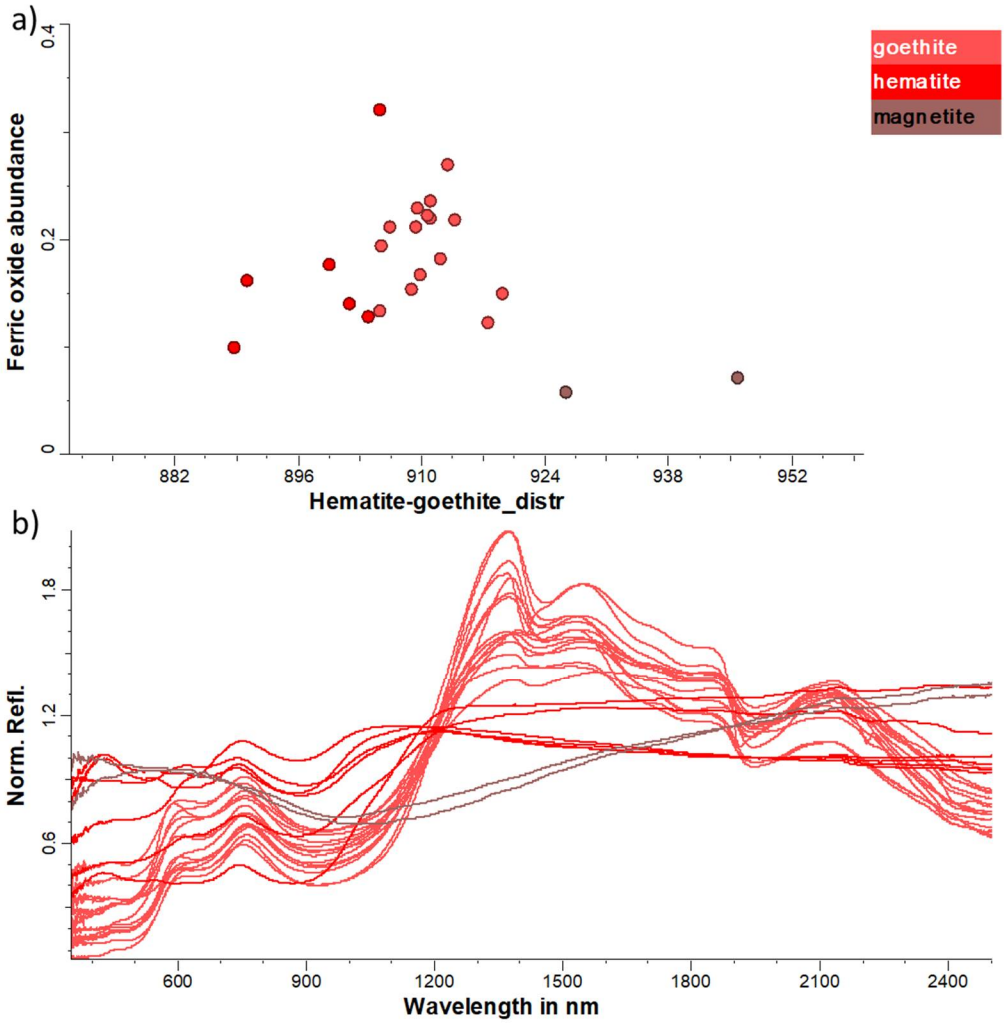

Figure 7 a) Wavelength position of the 900 nm crystal field absorption feature of ferric iron (Hematite-goethite distribution) on the x-axis plotted against the relative depth of said absorption feature on the y-axis, coloured by the mineral species; b) VNIR-SWIR reflectance spectra corresponding to samples plotted in a)

4.4 Hydroxyhalides

Figure 8 shows the VNIR-SWIR reflectance spectra of three atacamite minerals from the hydroxyhalide group. The reflectance spectra contain many trough features centred at 704, 872, 1469, 1855, 1993, 2160, 2342 and 2468 nm. The strong and right-hand asymmetric absorption in the 700 to 900 nm wavelength range stems from electronic transition bands related to divalent copper (centred at 672, 971 and 1179 nm). Absorptions in the 1400 nm and 1850 to 2500 nm wavelength range can be attributed to hydroxyl-related combinations of fundamental stretching and bending vibrations (Laukamp et al., 2015b).

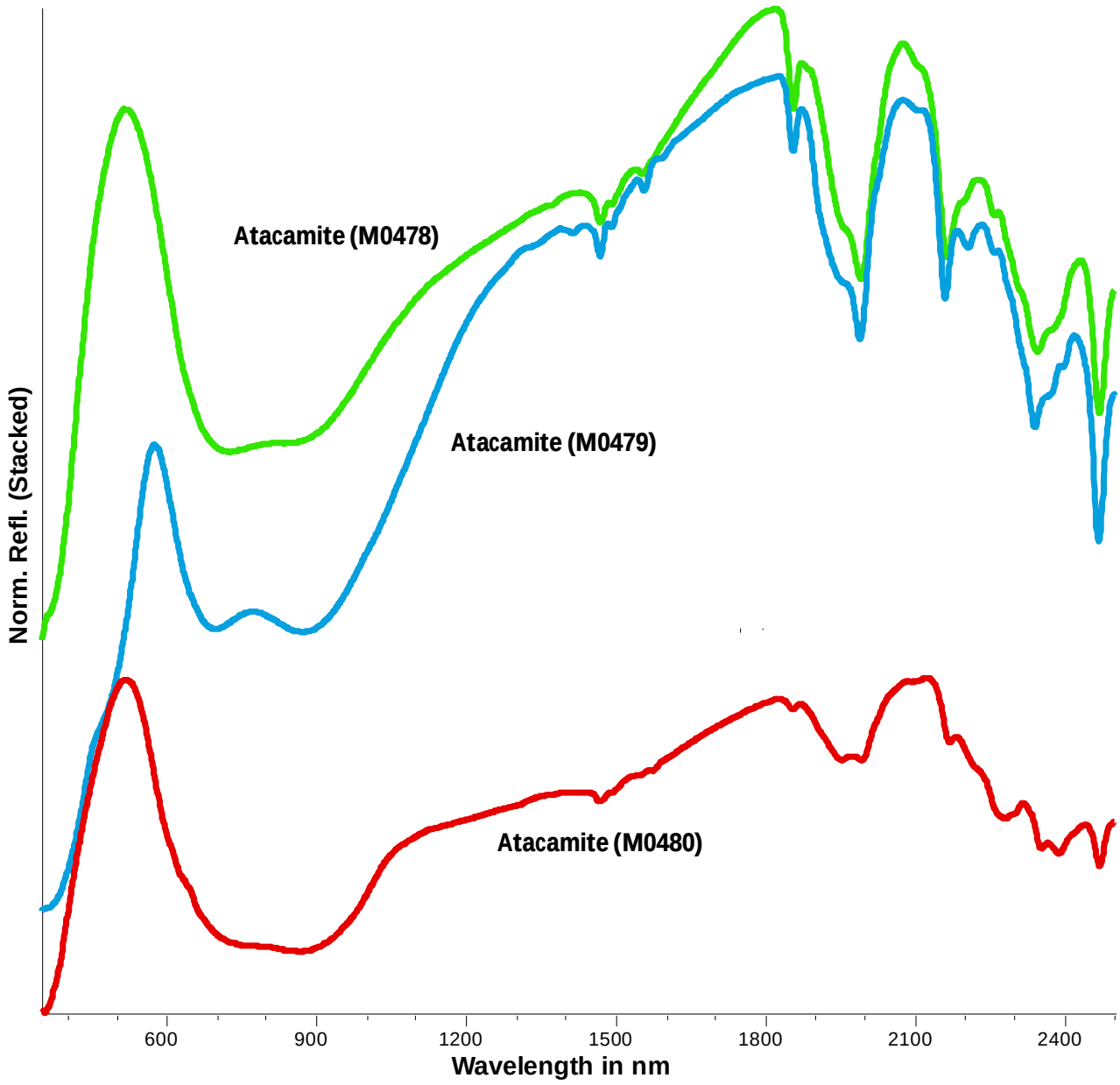

Figure 8 UV-VNIR-SWIR reflectance spectra (350 to 2500 nm) of hydroxyhalides.

4.5 Carbonates

Many different carbonate-based minerals were analysed from CSIRO's Mitchell Collection and Figure 9 displays the VNIR-SWIR reflectance spectra for twenty samples that seemed to be relevant and suitable in terms of the least number of impurities based on previous XRD and/or FTIR data. Although there were many carbonate-based minerals that were measured in the VNIR region, most of them contained common trough features at 1910 nm and 2355 nm. The wavelength position of these features shifted and varied significantly depending on the type of mineral. In the case of iron-related carbonates (i.e., siderite and ankerite), trough features were evident in the VNIR at 490 nm and 1050 nm. The ankerite also contained a weak trough at 1415 nm. The manganese-related carbonates (i.e., rhodochrosite) had troughs at 405, 445, 545, 1065 and 1335 nm, whereas for the nickel-related carbonates (i.e., gaspeite) features were found at 412, 680, 745 and 1190 nm. For the

copper-related carbonates (malachite and azurite) trough features were observed at <350, 840 and 1220 nm. In addition, the azurite mineral samples had strong trough features at 1500 and 2285 nm. By contrast, the rare earth element related carbonates such as bastnasite and parasite contained multiple trough features below 1200 nm (see chapter 5 for more details about REE-related absorption features in the VNIR), whereas a strong broad feature was observed for synchysite between 1000 to 1300 nm.

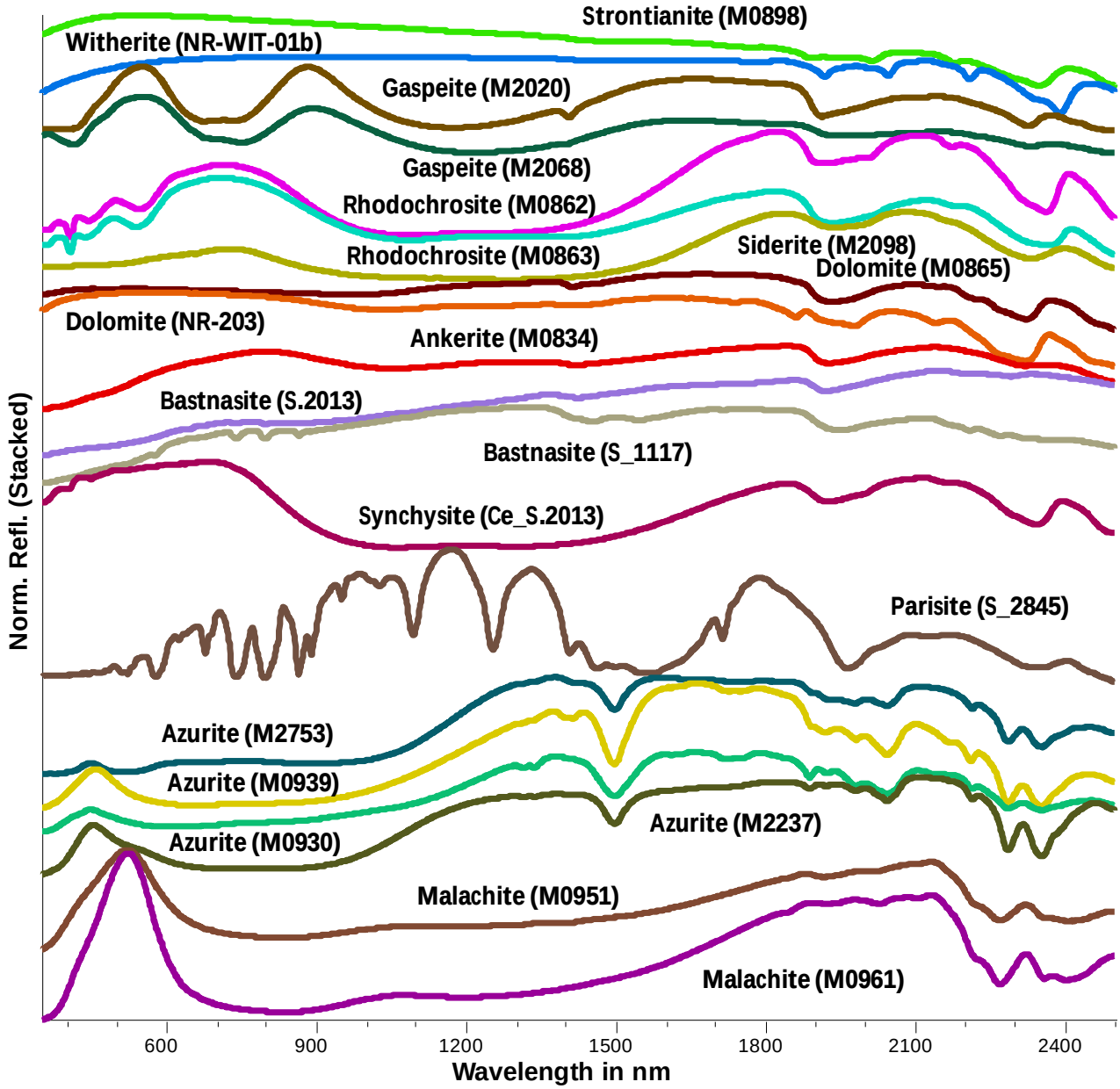

Figure 9 UV-VNIR-SWIR reflectance spectra (350 to 2500 nm) of selected carbonates.

4.6 Sulfates

Figure 10 shows the VNIR-SWIR reflectance spectra of two different jarosite minerals. The mineral jarosite is the only one that the VNIR-SWIR spectrum was recorded for the sulfate group. However,

the reflectance spectra contain a number of common trough features at <600, ~910 (broad), 1472, 1852, 2220 (shoulder) and 2267 nm. The sharp and small absorption at ~420 nm is consistent and diagnostic for jarosite. However, the 600 and 910 nm troughs are most likely attributed to the ferric iron.

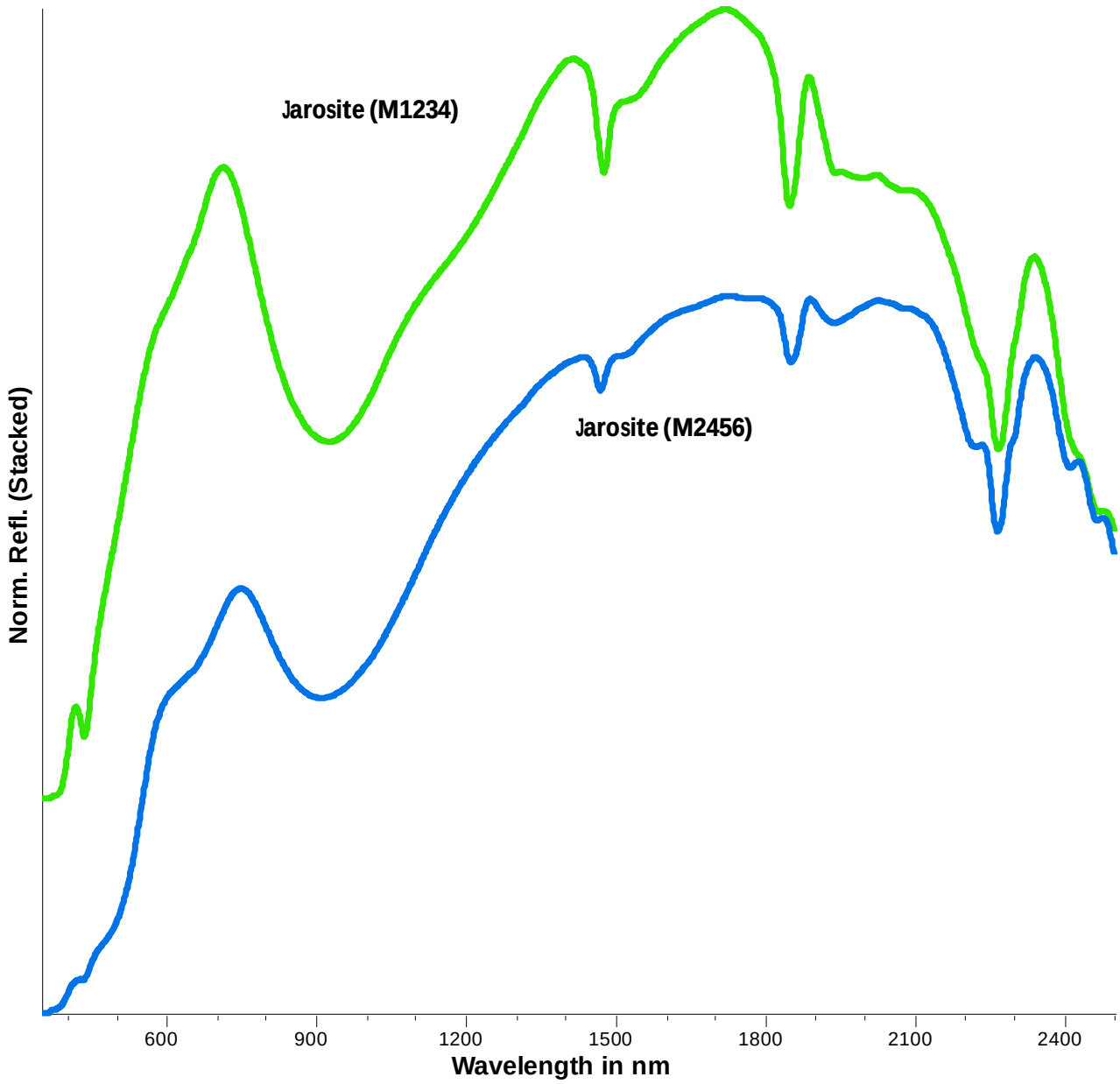

Figure 10 UV-VNIR-SWIR reflectance spectra (350 to 2500 nm) of anhydrous sulfates with OH or halogen.

4.7 Anhydrous phosphates

Figure 11 shows UV-VNIR-SWIR reflectance spectra of nominally anhydrous phosphates apatite, monazite and xenotime. Most absorption features shown in these reflectance spectra are due to REE-related electronic transitions (Table 8). A distinct triplet of absorption features at around 740

nm, 800 nm and 870 nm is mostly due to Nd, though Dy shows considerable overlap (Turner et al., 2014). These Nd-related absorption features are most prominent in monazite samples.

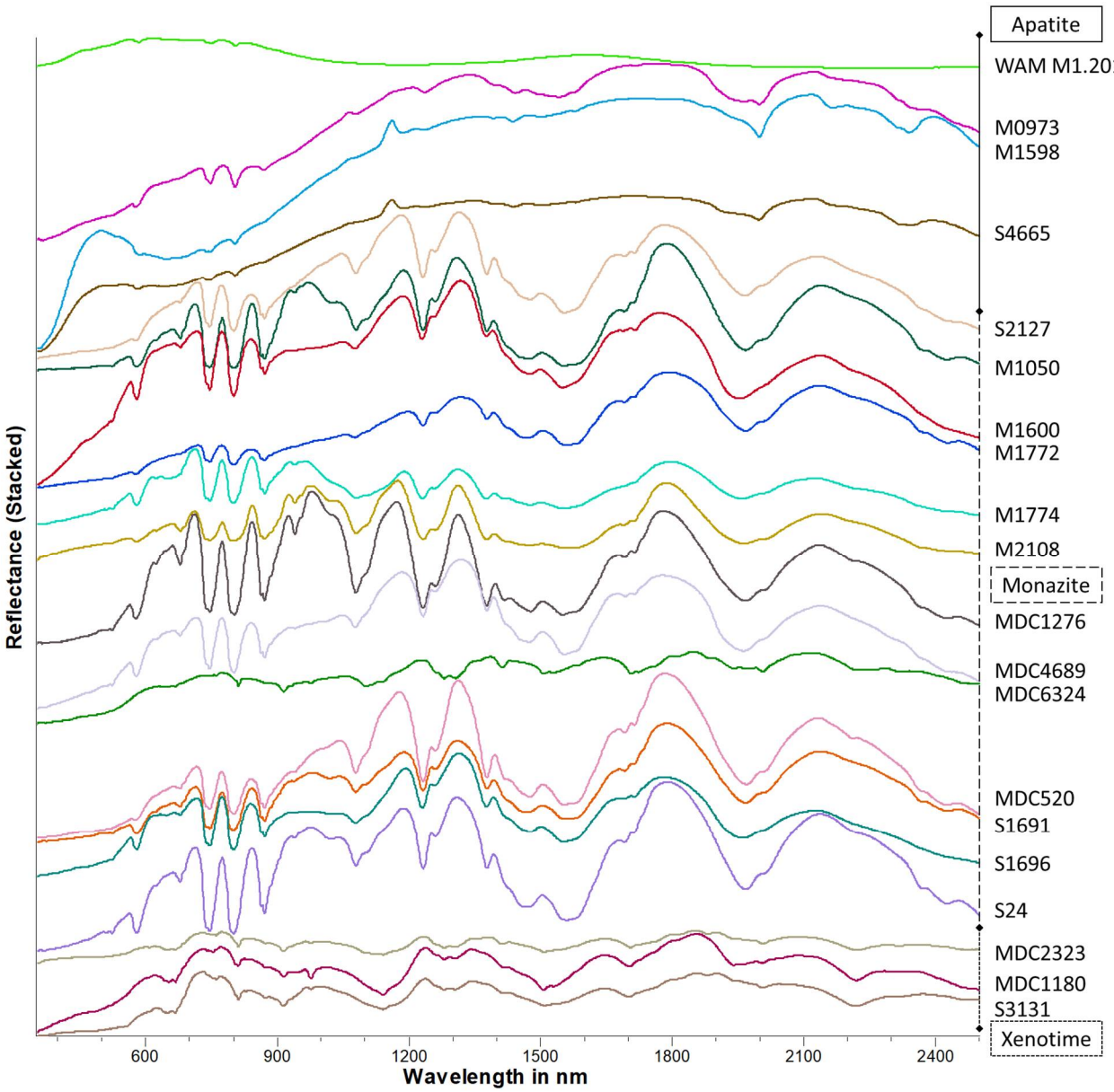

Figure 11 UV-VNIR-SWIR reflectance spectra (350 to 2500 nm) of apatite, monazite and xenotime.

Other strong REE-related absorptions prominent in monazite are potentially due to Sm (1075 nm, 1230 nm) and Er (978 nm). Absorption features in the SWIR can largely be attributed to REE/OH/PO4 (2364 nm). A full list of major absorptions in the investigated apatite, monazite and xenotime reference samples is given in Table 8. Figure 12 shows the UV-VNIR wavelength range of the phosphate reflectance spectra. Overall, the REE-related spectral signatures are distinctly different for each of the here presented types of phosphate minerals. Sample MDC6324 was classified as monazite by the sample provider. However, the UV-VNIR pattern matches xenotimes much better and further validation is required to determine its true mineral composition.

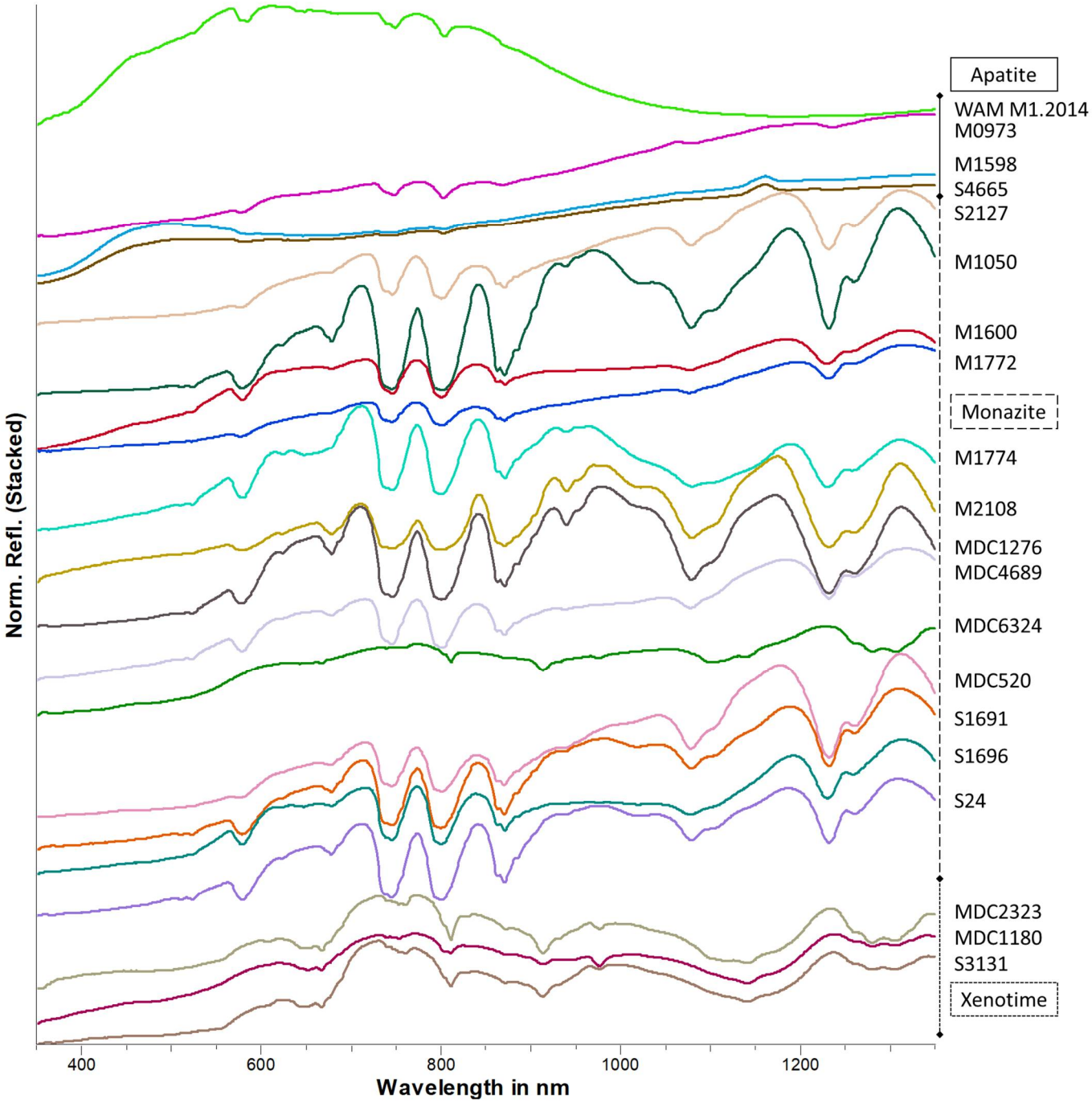

Figure 12 UV-VNIR reflectance spectra (350 to 1350 nm) of apatite, monazite and xenotime.

Table 8 (next page): UV-VNIR-SWIR absorptions of apatite, monazite and xenotime analysed for this report and compared with literature data and band assignments after Turner et al. (2014)

monazite				xenotime				fluorapatite		apatite	
Turner et al. (2014)		this work		Turner et al. (2014)		this work		Turner et al. (2014)		this work	
		523	w							526	wb
Nd	579	576	s					Nd	576	578	s
Nd	581	580	s					Nd	585	583	s
Nd	625	623	w			609	w				
				Ho>Er	643						
				Ho, Er, U^{4+}	653	653	m				
				Er>Ho	668	668	s				
Nd	679	678	s	Er>Ho, Nd	678	678	sh				
		688	sh	Tm > Nd	692	689	sh				
Nd	745	737	s	Dy>Ho, Nd?	740	740	w	Nd	738	738	m
		745	s	Dy>Ho, Nd?	748	748	w	Nd	749	749	s
				Dy>Ho, Nd?	754	753	m				
		794	s	Dy>Ho, Nd?	760	761	m	Nd	763		
		802	s	Dy>Er, Nd?	803			Nd	800		
Nd	800			Dy>Er, Nd?	811			Nd	805	803	s
Nd	863	862	s	Nd	872	872	w	Nd	870	870	wb
Nd	871	872	s								
		886	m								
		897	sh								
		907	sh	Dy, Yb, Ho	914	915	s				
						931	w				
Sm	941	940	m	Dy, Yb, Sm	951						
Sm	957	956	m	Dy, Yb, Sm	953	953	w				
				Yb, Er	977	977	m				
Yb>Er	980			Yb, Er	978						
Pr	1023	1015	wb								
Sm	1074	1078	s								
				Dy	1099	1099	mb				
Sm	1105	1107	m			1115	mb				
				Ho, Dy, U^{4+}	1143	1143	sb				
Sm	1232	1232	s			1172	sh	Sm	1232		
Sm	1257	1263	m			1258	m				
				Dy	1276	1289	s				
				Dy	1307	1307	s				
Sm	1377	1377	s			1361	w			1392	m
		1417	mb	H2O	1415	1412	m	H_2O	1433	1437	m
		1452	mb								
Pr	1471	1477	mb								
				Er>Sm, U^{5+}	1503	1506	s			1499	wb
Sm?	1553	1549	mb	Er>Sm	1528	1538	mb				
						1561	sh			1547	wb
		1584	mb			1588	mb			1579	wb
Dy, Nd	1691	1690	w	Dy	1704	1705	s				
Nd	1710	1716	w								
				Dy, Tb	1723	1726	m				
						1763	w				
						1813	w				
						1882	m				
Pr, Sm, H2O	1968	1943 to 1961	sb	Ho, Tb, H2O	1936	1937	s			1911	mb
						1962	m			1963	mb
						1979	m			1999	s
		2012	mb	Ho, Sm, Tb	2005	2006	s				
										2162	wb
				$REE/OH/PO_4$	2218	2217	sb				
						2260	sh				
						2315	w			2314	m
		2359	m							2341	mb
$REE/OH/PO_4$	2424	2422	m								
$REE/OH/PO_4$	2499			$REE/OH/PO_4$	2487	2456	wb				

4.8 Wolframite ($FeMnWO_4$) and Scheelite ($CaWO_4$) series

Figure 13 displays the UV-VNIR-SWIR reflectance spectra for wolframite and scheelite. The two scheelite samples had a trough centred around 1930 nm whereas the wolframites did not contain this band. In sample M1064, a weak feature was observed at around 1400 nm, suggesting that this absorption along with the feature at around 1900 nm are water-related, potentially pointing to impurities and/or fluid inclusions in this scheelite sample. All of the wolframite samples contained a broad and large tough feature between 1200 to 1900 nm, which can mainly be attributed to electronic transitions related to Fe and/or Mn. The reflectance for all the mineral appeared to decrease below 700 nm and this feature/band was relatively broad. Tungsten probably has a considerable contribution to the strong absorption in the UV, though iron plays a major role in the wolframite in this case too.

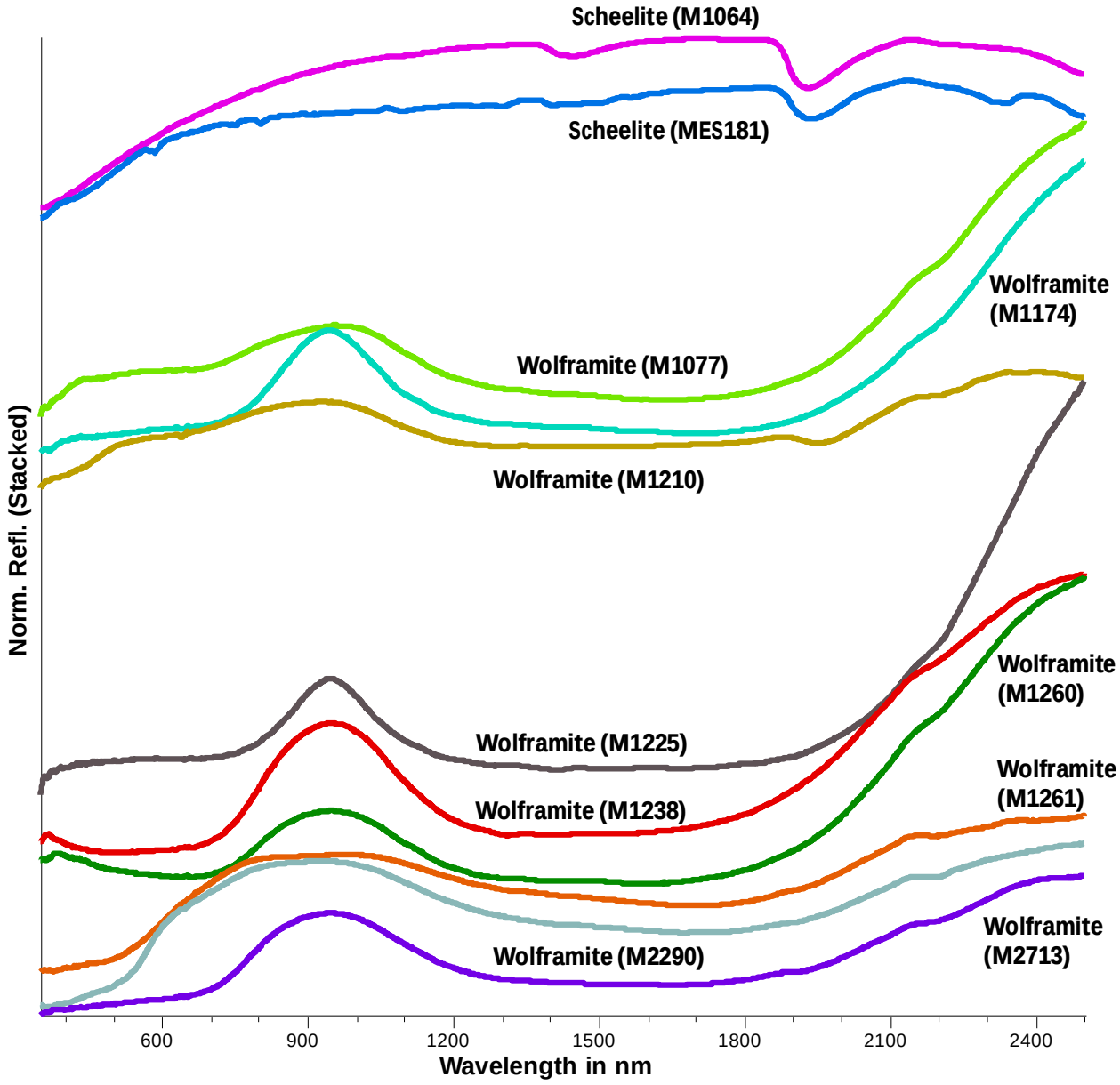

Figure 13 UV-VNIR-SWIR reflectance spectra (350 to 2500 nm) of selected wolframite and scheelite minerals.

4.9 Nesosilicates I – phenakite and olivine group

Figure 14 displays a range of nesosilicates (i.e., phenakite and olivine groups). The UV-VNIR-SWIR reflectance spectra for all olivine reference samples looked almost the same, noting that the broad feature at ~1000 nm was present in all five olivine samples that were measured. In addition, a trough feature around 450 nm was evident and is probably associated with electronic transitions of iron. A weak band at ~635 nm was also observed but this feature was not evident in the willemite sample. However, the reflectance for the willemite sample decreased significantly below 650 nm and is probably associated with electronic transitions of the zinc ion.

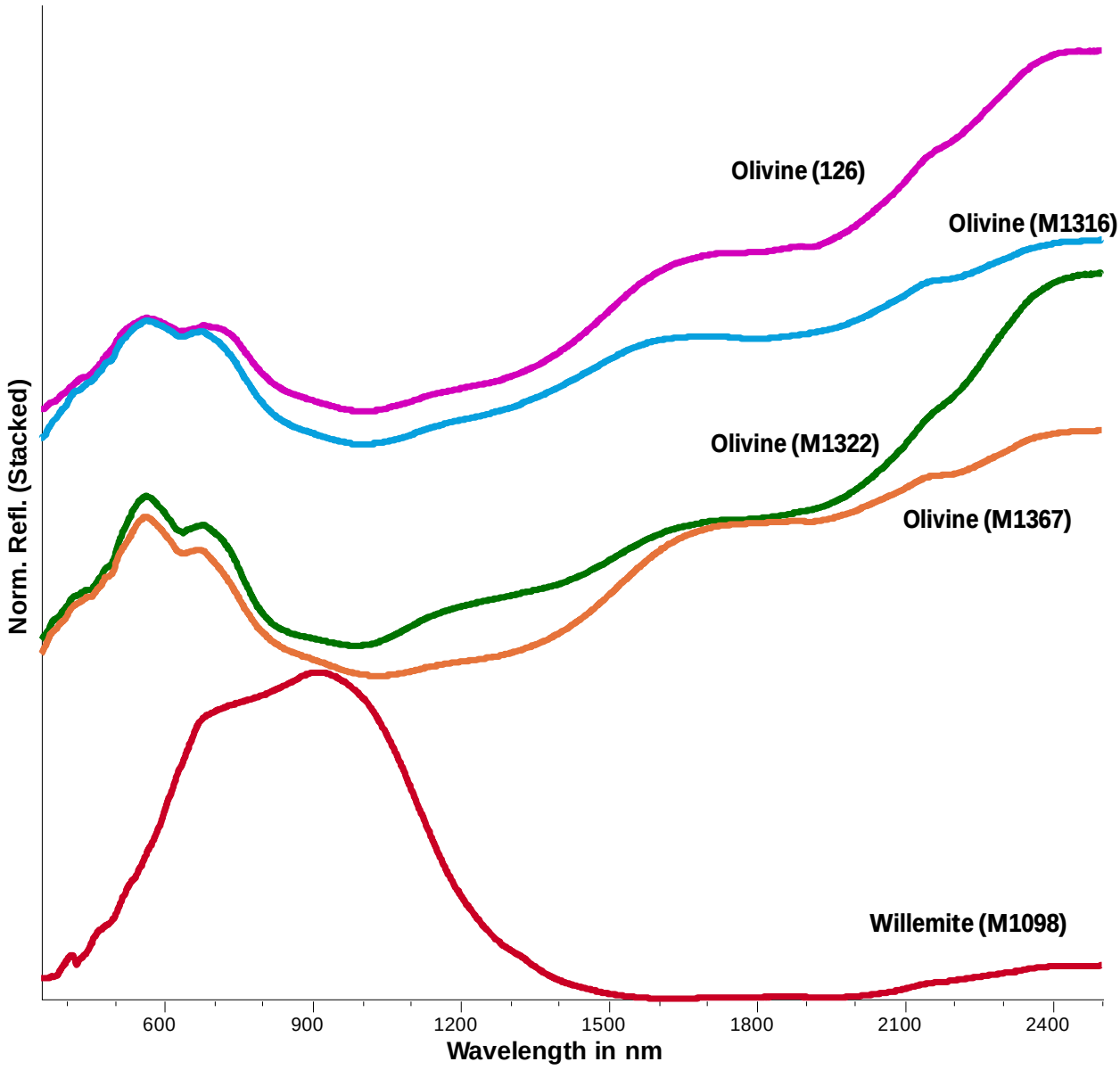

Figure 14 UV-VNIR-SWIR reflectance spectra (350 to 2500 nm) of selected phenakite and olivine minerals.

4.10 Nesosilicates II – garnet group

Figure 15 displays the UV-VNIR-SWIR reflectance spectra for a range of nesosilicates (i.e., garnet group). In general, the pyrope samples generated a slightly different reflectance spectrum compared to the other garnets, noting a broad and intense peak between 600 to 1150 nm. Similarly, the uvarovite samples displayed three intense trough features at 350, 450 and 620 nm. In most cases, the reflectance for the nesosilicates were relatively low around 400 nm and the reflectance generally decreased from 600 to 350 nm. Interestingly, a trough feature was observed between 850 to 890 nm for the grossular, andradite and garnet (M1328) samples. The garnet sample M1413 had multiple weak trough features at 495, 570, 700 nm and this was not observed for the other garnet (M1328).

Representatives of garnet in the VNIR SRL 2.0 comprise a wide compositional range, including almandine ($Fe_3Al_2(SiO_4)_3$), andradite ($Ca_3Fe_2(SiO_4)_3$), grossular ($Ca_3Al_2(SiO_4)_3$), pyrope ($Mg_3Al_2(SiO_4)_3$), spessartine ($Mn_3Al_2(SiO_4)_3$), uvarovite ($Ca_3Cr_2(SiO_4)_3$) and additional unspecified garnets. According to some reports (Izawa et al., 2018), reflectance spectra of common silicate garnets typically contain an envelope of strong features at ~1300, ~1700, and ~2300 nm due to spin-allowed transitions of Fe^{2+} and numerous weaker features at shorter wavelengths (~400 to 800 nm) due to spin-forbidden transitions of Fe^{2+} and Fe^{3+}. Reflectance spectra of garnet containing significant Fe^{3+} display a marked red spectral slope in the ultraviolet and visible due to Fe–O metal–oxygen charge transfer processes. Metal–metal intervalence charge transfer processes produce broad features in reflectance spectra of garnets, with features due to Fe^{2+} and Fe^{3+} transitions typically in the ~400 to 500 nm range, and those due to Fe^{2+} and Ti^{4+} transitions in the 410 – 460 nm range. Reflectance spectra of Mn-bearing garnet (e.g. spessartine) have additional weak features near 410 nm that are ascribable to spin-forbidden transitions of Mn^{2+}. Cr-bearing garnet spectra have additional strong and distinctive spectral features due to Cr^{3+} spin-allowed features near 400 to 410 nm and 560 to 620 nm and Cr^{3+} spin-forbidden near 700nm.

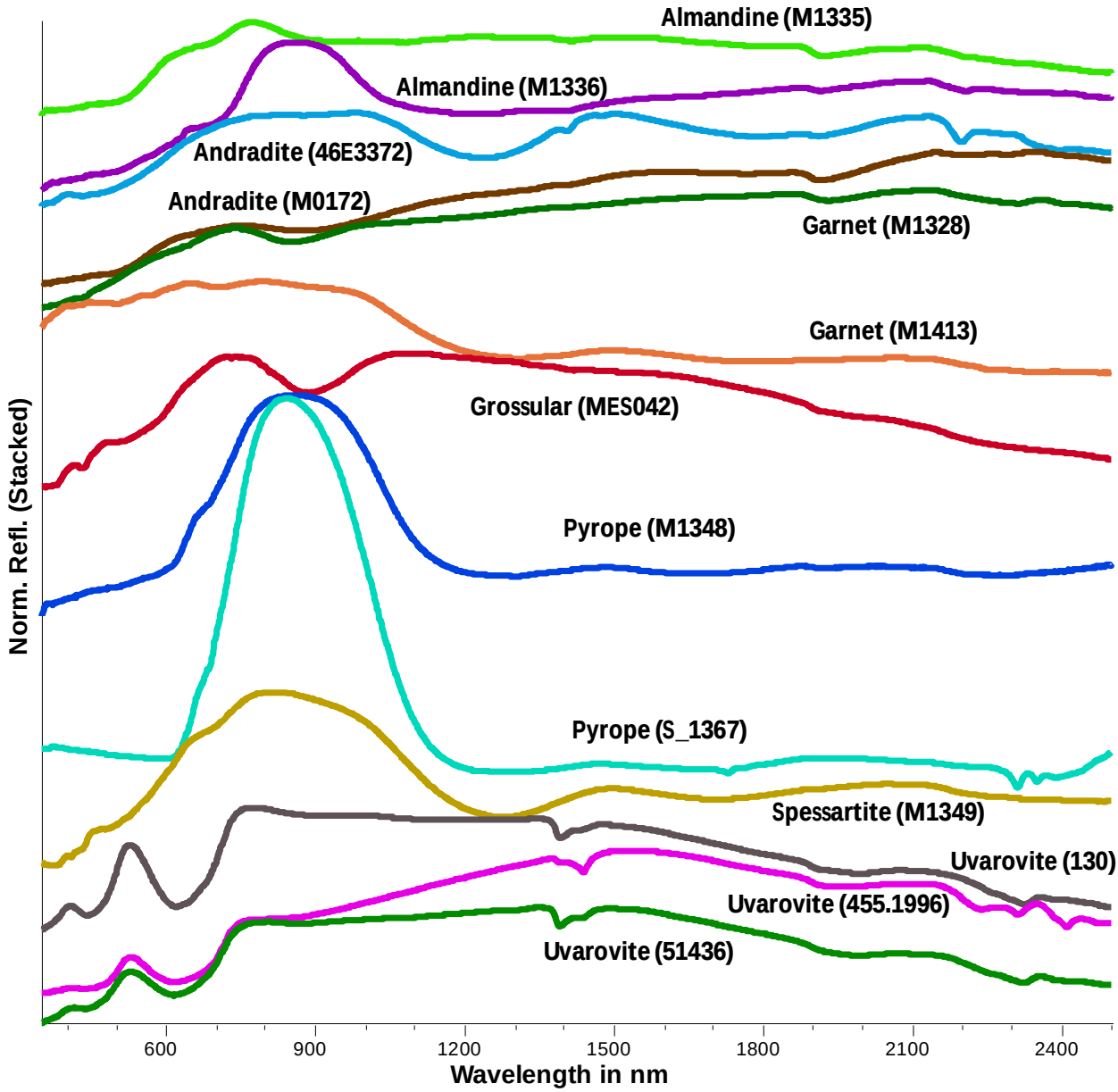

Figure 15 UV-VNIR-SWIR reflectance spectra (350 to 2500 nm) of selected garnet minerals.

4.11 Nesosilicates III – silicate apatites

Figure 16 displays the UV-VNIR-SWIR reflectance spectra for two different britholite samples, part of the silicate apatites. One of them contained many trough features compared to the other sample. For instance, numerous sharp and intense trough features were observed for the britholite sample MDC3386 and these occurred at 585, 747, 804, 877, 1080, 1226, 1380 and 1500 nm. For britholite MES107 a broad trough feature occurred between 900 to 1200 nm. A closer look at the reflectance spectrum of britholite MES107 revealed very weak troughs at 642, 799, 985 and 1099 nm. In both cases, the reflectance values decreased from 650 to 350 nm. Britholite is a REE-bearing silicate apatite ($X_5(SiO_4,PO_4)_3(OH,F)$ with X = Ce, Ca, Th, La, Nd). The sharp absorptions in sample MDC3386 can be attributed mainly to Nd. The reason for the subdued REE-features of sample MES107 is unclear at the stage, but might be due to the very small size of the britholite amongst the host rock.

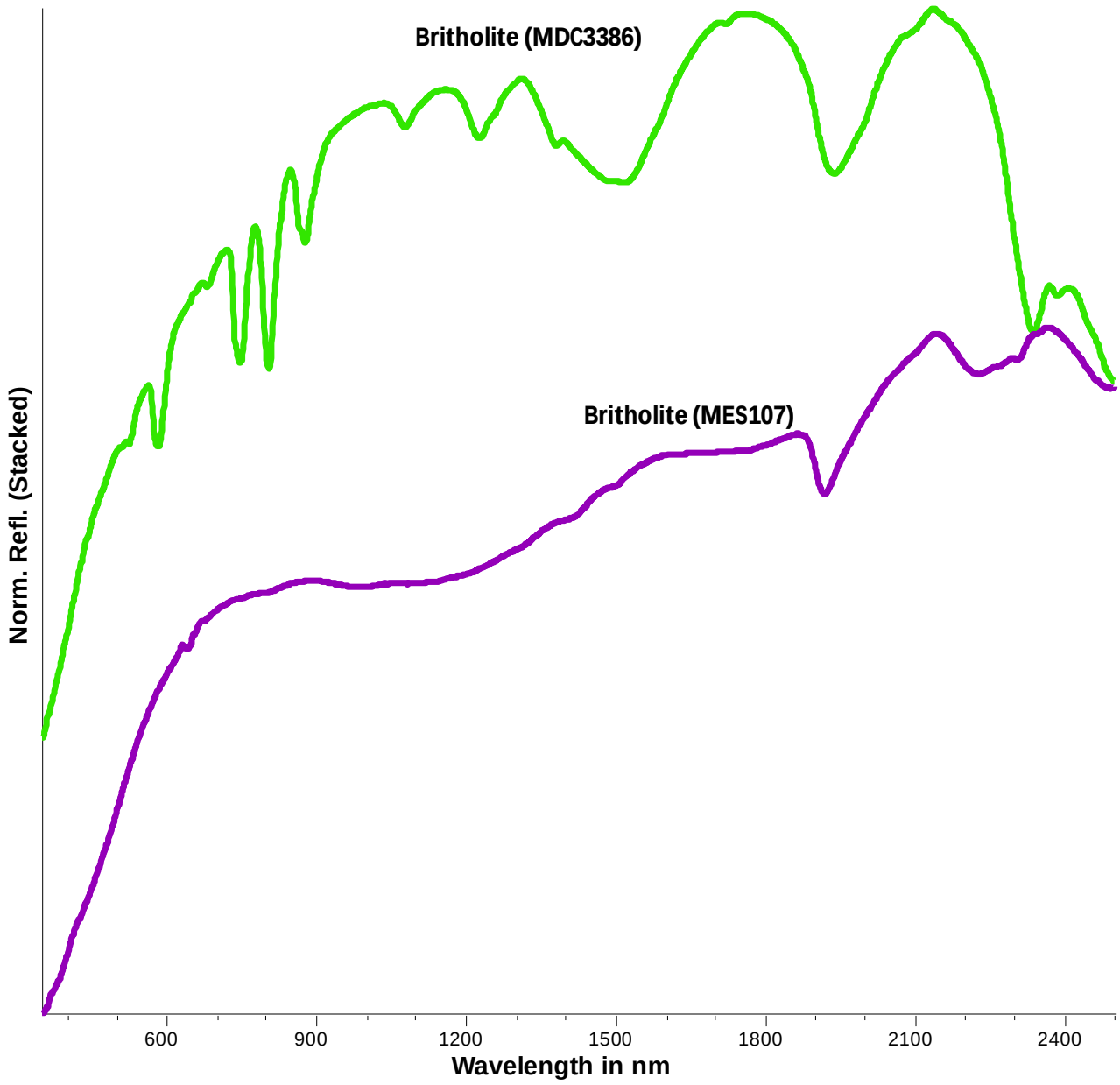

Figure 16 UV-VNIR-SWIR reflectance spectra (350 to 2500 nm) of selected silicate apatite minerals.

4.12 Sorosilicates – epidote group

Epidote is a calcium aluminium iron sorosilicate mineral that is an abundant rock-forming mineral, but one of secondary origin. It is commonly a shade of green colour and occurs in marble and schistose rocks of metamorphic origin and is also a product of hydrothermal alteration. The reflectance spectra of sorosilicate minerals were measured and Figure 17 shows the UV-VNIR-SWIR reflectance spectra. The epidote samples all contained the following trough features at 470, 620, 1045, 1545, 1832, 1951, 2254 and 2340 nm. The reflectance generally deceased between 600 to 320 nm for all samples. In epidote, the main features in the 450 to 1100 nm wavelength range are largely due to electronic transitions associated with Fe^{3+}. The SWIR absorptions are overtones and combinations of hydroxyl-related vibrational modes (Langer and Raith, 1974). The epidote series comprises a solid solution series ranging from clinozoisite (Ca2Al3Si3O12(OH)) to pistasite

(Ca2Fe3+Al2Si3O12(OH)) as the two endmembers of the $AlFe^{3+}_{-1}$ solid solution. Each OH group in epidote is bonded to two M sites, which are occupied by varying amounts of Al and Fe^{3+}. Hydroxylated sorosilicates of the epidote series are characterised by absorptions in the 1545 to 1563 nm wavelength range, which are also due to 2vOH.

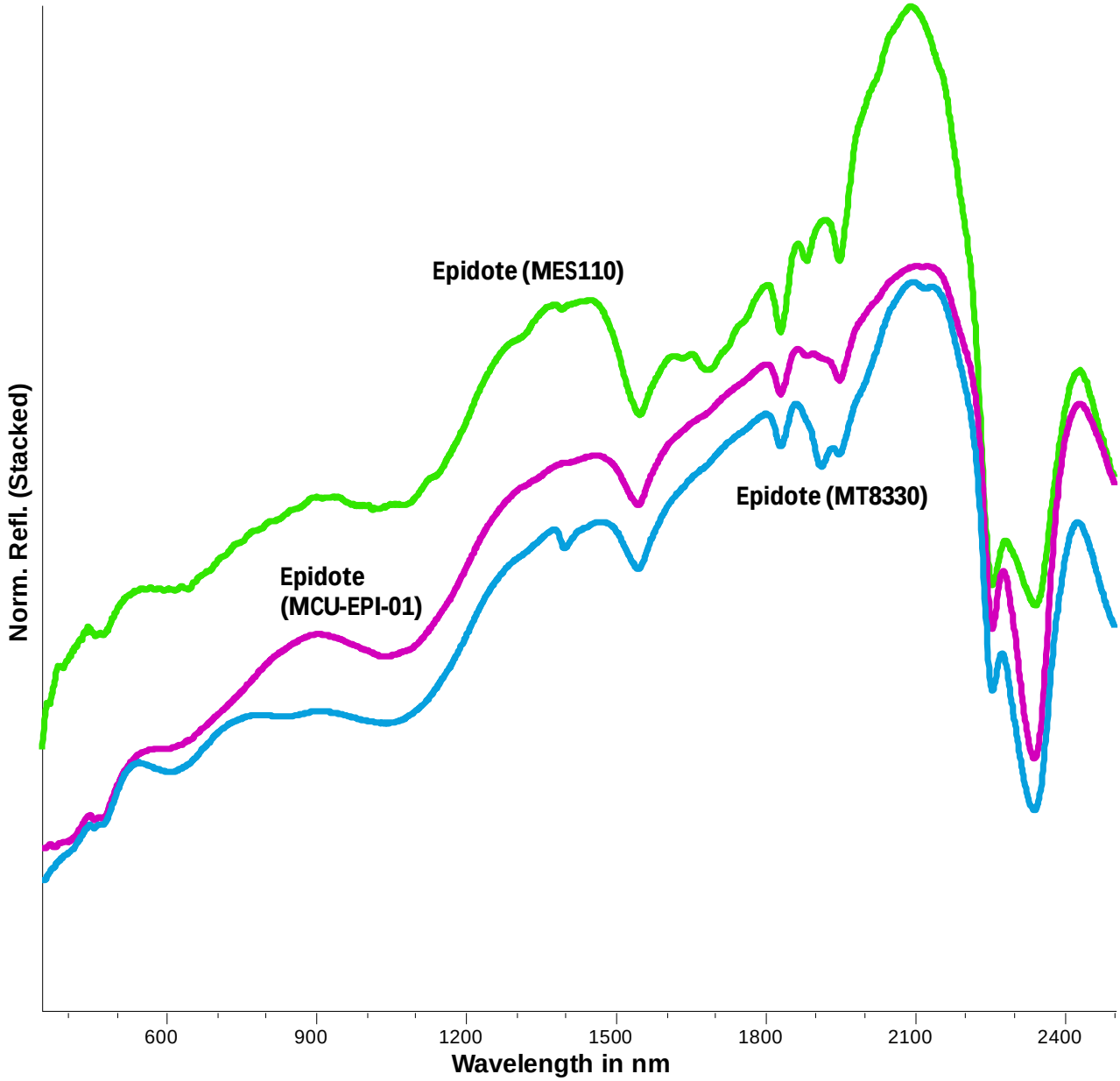

Figure 17 UV-VNIR-SWIR reflectance spectra (350 to 2500 nm) of selected epidote minerals.

4.13 Cyclosilicates – tourmaline and eudialyte group

Figure 18 shows the UV-VNIR-SWIR reflectance spectra of tourmalines and eudialyte, which are part of the cyclosilicates. The reflectance spectra for most of the tourmalines (with the exception of tourmaline M1361) looked almost the same in that three major broad absorptions occur in the UV-VNIR wavelength range. In addition, a number of sharp trough features were evident at 2207, 2246,

2303 and 2370 nm, which can all be attributed to hydroxyl-related combination bands that are different in intensity depending on the cation composition of the respective tourmaline. Eudialyte is a REE-bearing cyclosilicate ($Na_4(Ca,Ce)_2(Fe^{2+},Mn,Y)ZrSi_8O_{22}(OH,Cl)_2$) and sample MES111 displays strong REE-related absorptions at around 740, 800, 1270 and 1550 nm. The distinct 1930 nm trough and the associated feature at around 1400 nm can be both attributed to water.

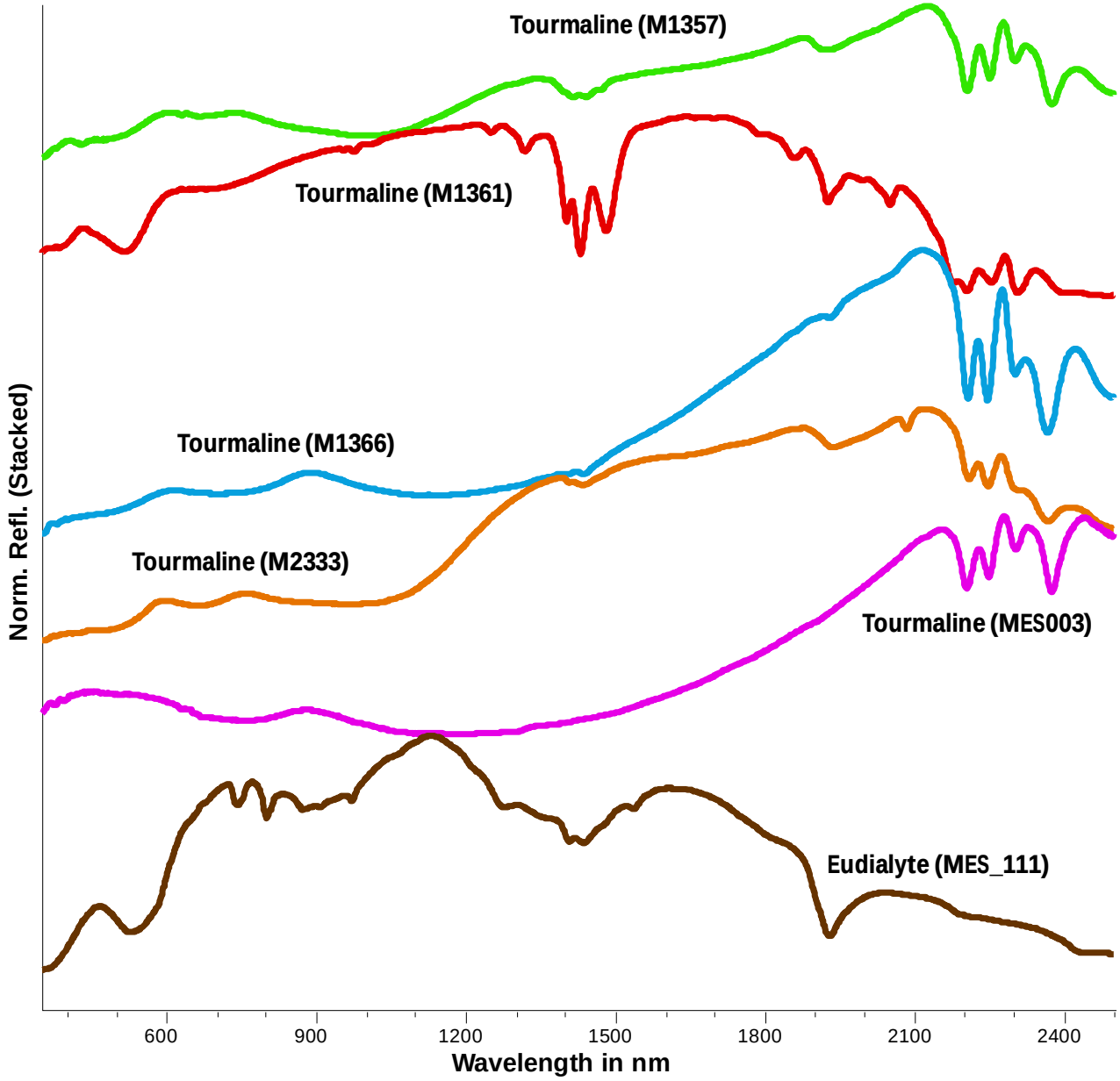

Figure 18 UV-VNIR-SWIR reflectance spectra (350 to 2500 nm) of selected tourmaline and eudialyte group minerals.

4.14 Inosilicates – pyroxene group

The reflectance spectra of many minerals from the pyroxene group were measured and Figure 19 shows the UV-VNIR-SWIR reflectance spectra. The reflectance spectra for the enstatite samples were similar with a broad trough feature observed at 925 nm, which can be attributed to iron. The geochemical analysis of enstatite sample MES041 indicates a low iron content (Table 5), suggesting

that also the other two enstatite samples don't have the endmember enstatite composition ($Mg_2Si_2O_6$). In the SWIR, troughs were also evident at 1395 nm, 1900 nm and 2316 nm, indicating alteration of the nominally anhydrous enstatites. In the case of the hedenbergite samples ($CaFe^{2+}Si_2O_6$) a broad trough feature occurred at 1065 nm, which can be attributed to ferrous iron. In the case of diopside ($CaMgSi_2O_6$), a broad trough feature was also observed but varied between 1000 to 1100 nm, confirming the iron reported in the geochemical analyses (Table 5). As for the augite ($(Ca,Mg,Fe)Si_2O_6$) samples, the VNIR spectra show a peak at around 600 nm associated with lower reflectance in the 750 to 1200 nm wavelength region, which again can be largely attributed to iron. Sample (M2197) contained multiple trough features at 800, 1000 and 1220 nm. Despite some distinct differences between the various types of minerals, the reflectance of all pyroxene group minerals generally deceased between 600 to 320 nm. Aegirine ($NaFe^{3+}Si_2O_6$) sample MES085 is different to other pyroxene samples, in that a potentially Nd-related triple feature occurs in the 740 to 870 nm wavelength range, indicating impurities.

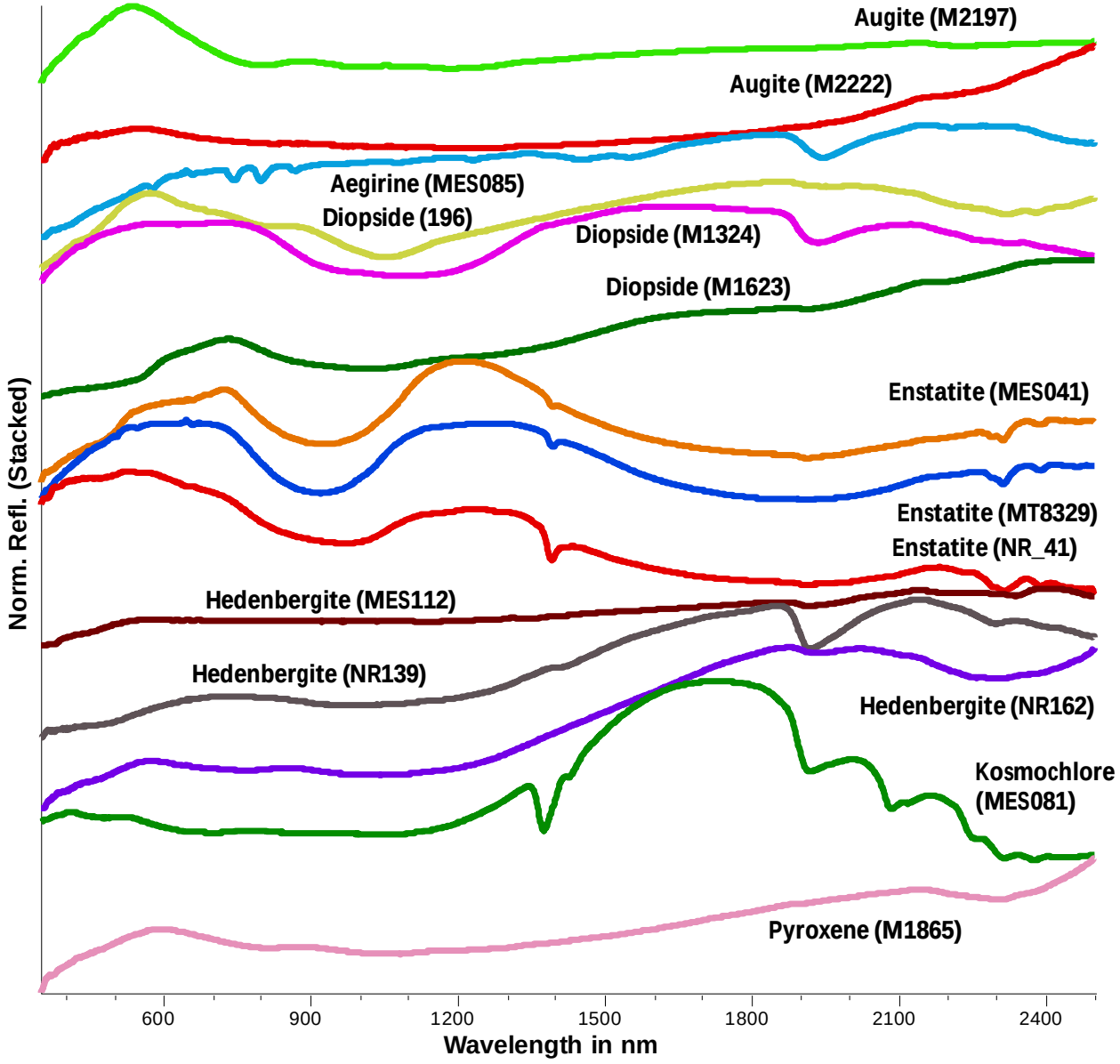

Figure 19 UV-VNIR-SWIR reflectance spectra (350 to 2500 nm) of selected pyroxene group minerals.

4.15 Inosilicates – pyroxenoid group

Figure 20 displays the UV-VNIR-SWIR reflectance spectra of various rhodonite (Mn_2SiO_3) and pyroxmangite ($(MnFe^{2+})SiO_3$) minerals. The general shape of the VNIR reflectance spectrum was almost similar in all cases. For instance, a peak between 600 to 900 nm was observed and the reflectance values were lowest between 900 to 1200 nm, but especially in the rhodonite sample M1094 decreasing towards 2500 nm. The overall SWIR low reflectance is potentially due to the high Mn-content of the rhodonite. The 1034 nm trough feature was broad and the position varied slightly and can be attributed to iron. All samples contained additional trough features at 412 and 540 nm.

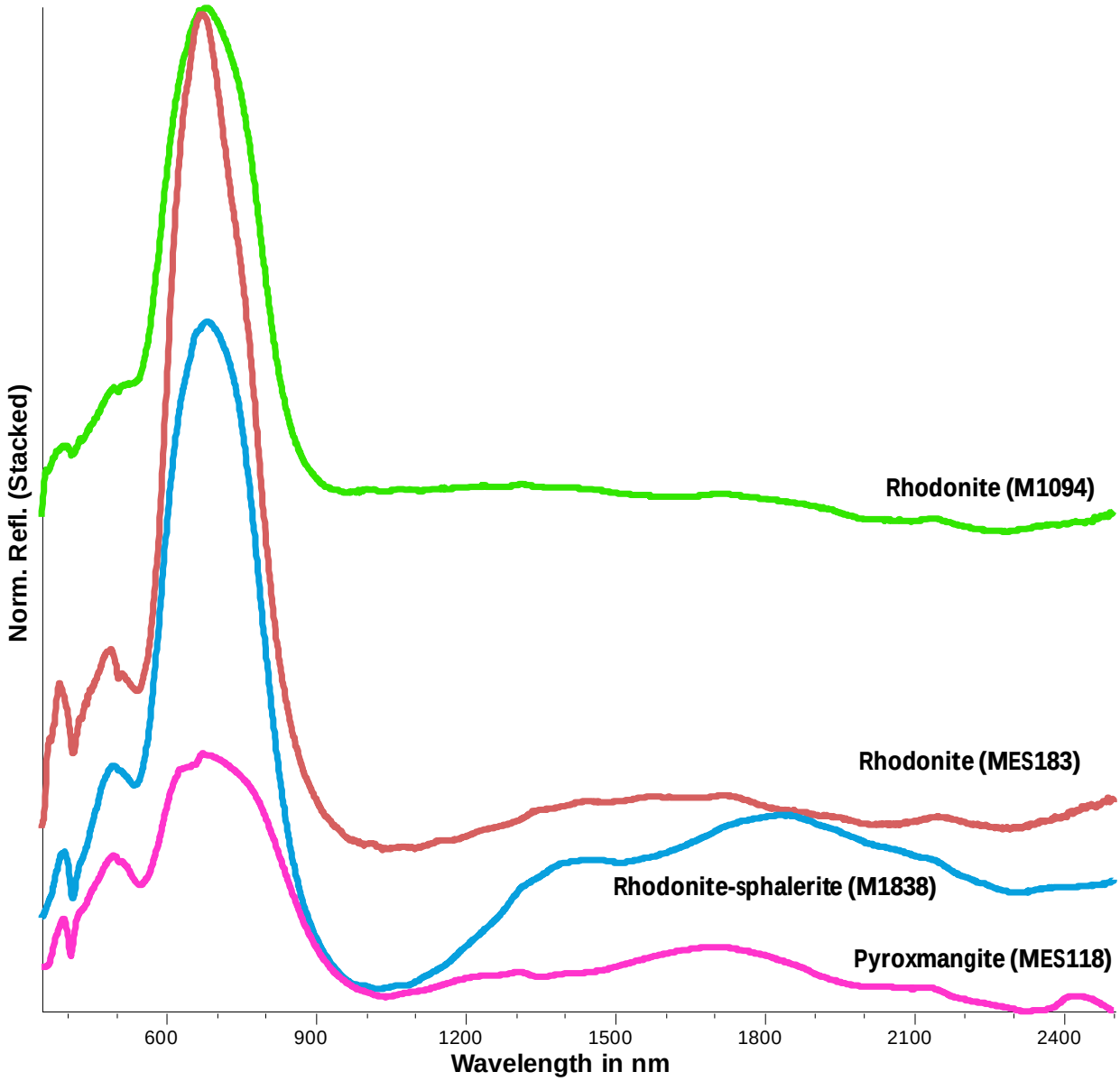

Figure 20 UV-VNIR-SWIR reflectance spectra (350 to 2500 nm) of selected pyroxenoid and pyroxmangite group minerals.

4.16 Phyllosilicates - micas

Figure 21 displays the UV-VNIR-SWIR reflectance spectra for a range of different micas which belong to the group of phyllosilicate minerals. The VNIR spectra for the four biotite samples that were measured show a distinct slope increasing from about 1000 to 2000 nm. The strong absorption in the VNIR wavelength region can be attributed to iron in biotite. In the case of sample M1593, two weak trough features at 880 and 1150 nm were evident and these are probably ferrous-related crystal field absorptions (CFA) in biotite (Burns, 1993). Similarly, samples Erwan1, M1589 and MES001 had very weak trough features at 715, 910 and 1115 nm, which can all be attributed to iron-related CFAs. The reflectance of all biotite samples decreased below 380 nm and this probably arises from the formation of a trough feature located in the UV. The fuchsite sample comprised many trough features at 420, 615, 1415, 2213, 2350 and 2450 nm. In addition, the green reflectance is high at 550 nm. As for phlogopite (MES014), the sample had prominent features at 715, 888, 1053, 1378, 1921, 2246, 2328, 2382 and 2246 nm, with VNIR absorptions mainly due to iron. The VNIR absorptions in fuchsite 193 sample at 420 nm and 615 nm can be attributed to Cr^{3+} and/or Fe^{3+}-related CFAs (Burns, 1993).

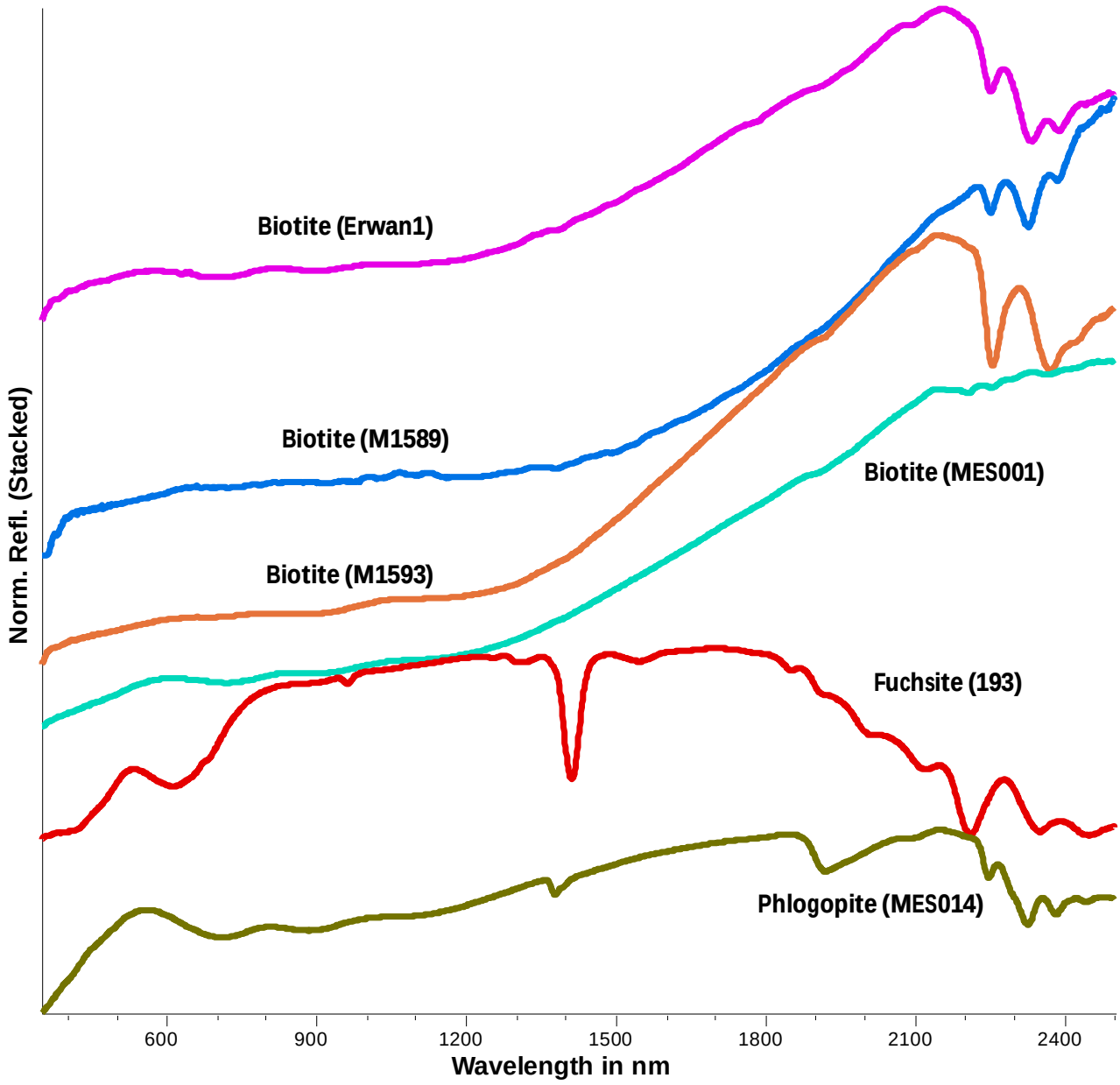

Figure 21 UV-VNIR-SWIR reflectance spectra (350 to 2500 nm) of selected biotite and muscovite subgroup minerals.

4.17 Phyllosilicates - garnierite

Figure 22 displays the UV-VNIR-SWIR reflectance spectra of two garnierite-bearing samples, which looked similar. At least six significant trough features were evident at 390, 665, 1130, 1408, 1912 and 2322 nm. In addition, the peak at 566 nm which gives it a green colour, was broad and asymmetrical. The VNIR absorptions are mainly due to Ni but also ferric iron. The SWIR absorptions can be attributed to hydroxyl- and water-related combination and overtone bands of fundamental stretching and/or bending vibrations in the mid and thermal infrared.

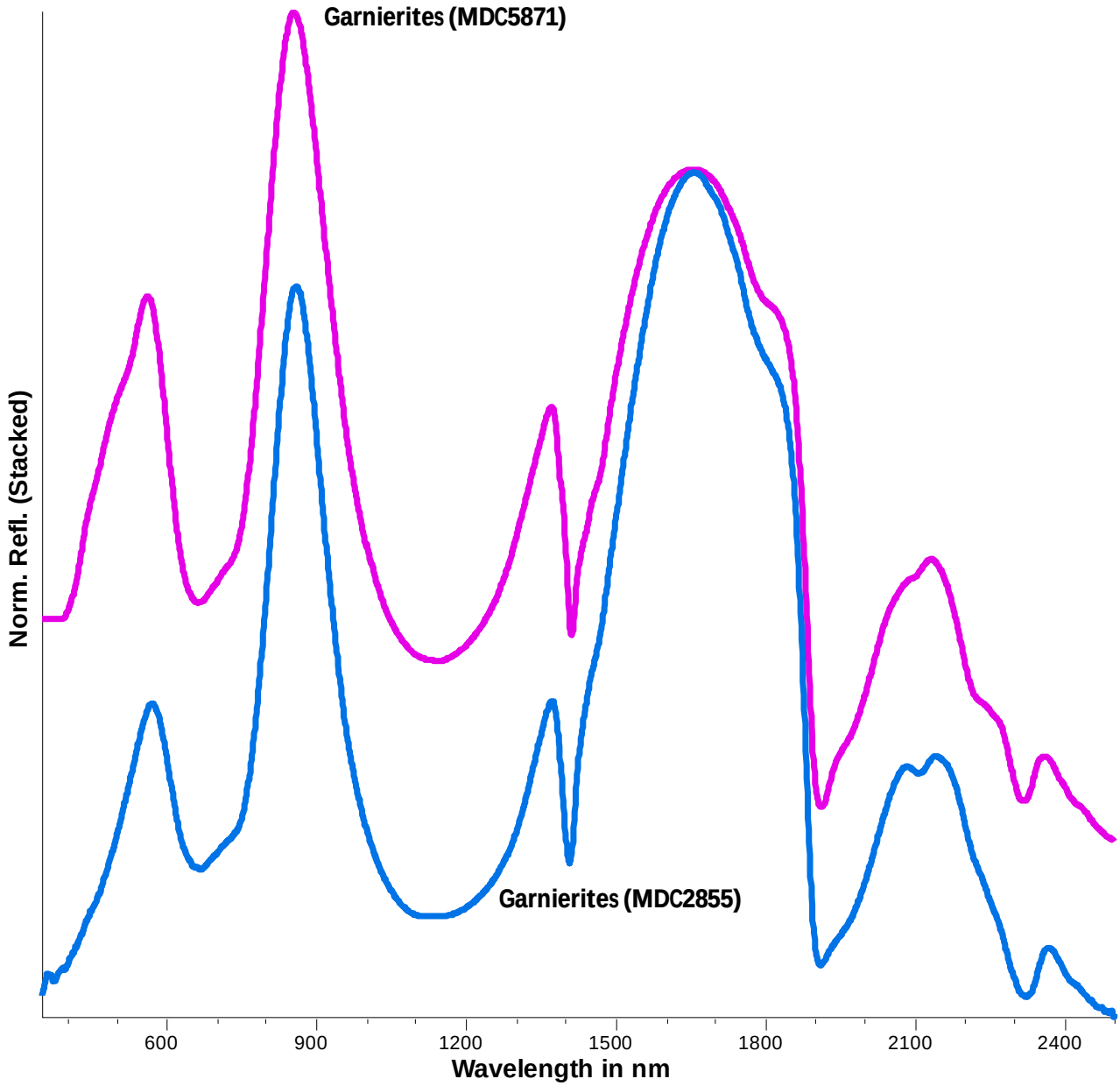

Figure 22 UV-VNIR-SWIR reflectance spectra (350 to 2500 nm) of garnierites.

4.18 Phyllosilicates - chrysocolla

Figure 23 displays the UV-VNIR-SWIR reflectance spectra of five chrysocolla-bearing samples, noting that the reflectance spectra looked almost identical. All of them contained a broad, right asymmetric and intense trough feature at 750 nm that is due to the broad CFAs of Cu^{2+} centred at 714 and 847 nm, except for sample M1646. In the case of sample M1646, it comprised two features at 677 nm and 867 nm, suggesting a partial replacement of Cu^{2+} by another transition metal. The SWIR absorption features were observed at 1417, 1791, 1914 and 2271 nm and can be attributed to hydroxyl- and water-related combination and overtone bands of fundamental stretching and/or bending vibrations in the mid and thermal infrared.

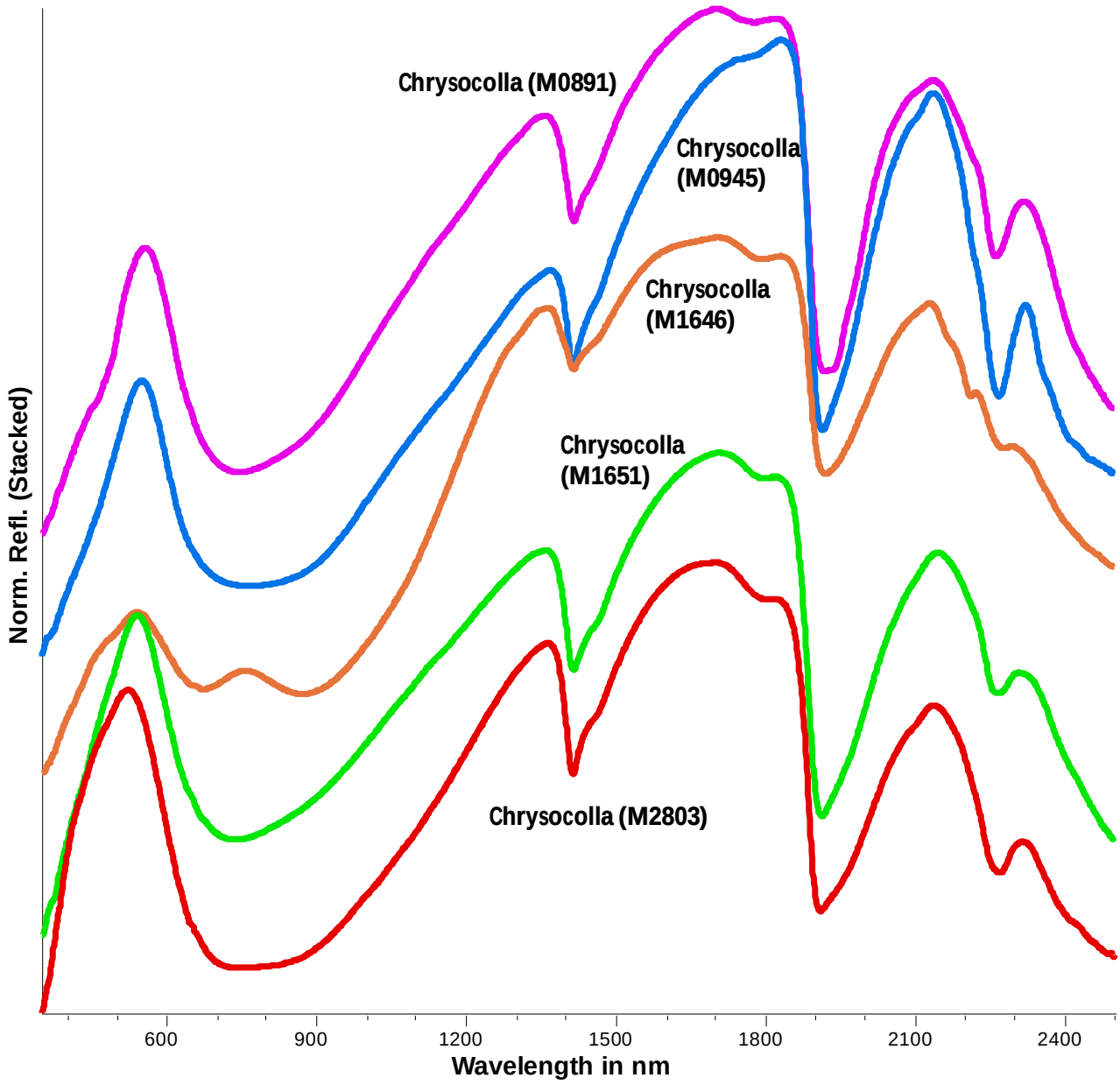

Figure 23 UV-VNIR-SWIR reflectance spectra (350 to 2500 nm) of selected chrysocolla group minerals.

5 Summary of VNIR-active REE absorptions and scripts

The increased interest in critical metals in REEs has recently triggered more research in the band assignments of REE-related electronic modes and the spectral signatures of the REE-bearing host minerals (Lorenz et al., 2018; Morin Ka, 2011; Turner et al., 2018, 2016, 2014). This section aims to 1) summarise some of the stronger and more distinct electronic modes associated with REEs hosted in carbonates and phosphates, and 2) introduce a range of feature extraction scripts that can be used to track the respective REEs in reflectance spectra obtained with field or drill core sensing instruments. Electronic absorption processes in trivalent REEs lead to sharp absorption features in the UV, VNIR and SWIR wavelength regions (Adams, 1965; Fassel, 1961). For example, Neodymium (Nd) has characteristic absorption bands at the following wavelengths: 420, 475, 525, 580, 740, 800, 870 nm (Rowan et al., 1986). Because of their electronic configuration, La_2O_3, Lu_2O_3 and CeO_3 do not show these electronic absorption features and are *not active* in reflectance spectra (White, 1967). A detection limit of 300 ppm for successful identification of Nd using hyperspectral data from a laboratory setup was postulated (Rowan et al., 1986). However, electronic absorption bands of ferric iron and/or other transition metals in, for example, iron oxides or carbonates may sometimes partially or fully mask some or all REE-related absorption features of concern.

Table 9 summarises the wavelength centre positions of selected carbonates (bastnäsite, parasite and synchisite) and phosphates (monazite, xenotime, fluorapatite and apatite) that were described in the recent literature and that were observed in the course of this study. From this, it can be observed that the same REEs produce absorptions features in carbonates and phosphates over a similar wavelength range. However, the centre wavelength position of the respective REE depends on the host mineral and, more specifically, on differences of the coordination polyhedra for the REE cations between the respective crystal structures (Turner et al., 2016). Nd produces a strong absorption in bastnaesite, parasite and synchisite at 740 or 741 nm. However, in monazite and apatite, the same electronic mode is positioned at 745 and 749 nm, respectively. Even a 5 nm difference of absorption feature wavelengths can be reliably determined in current hyperspectral field and drill core sensors. Therefore, this provides the exploration geologist with a cost-effective tool for the identification of the REE species and the host mineral.

Sixteen feature extraction scripts have been used to determine the relative intensity or depth ("D") and the wavelength position ("W") of a given REE-related absorption feature. All scripts apply a three-band polynomial fit around the band with the lowest reflectance where the background hull is removed by division. It should be noted that the relatively low polynomial degree leads to a clustering of samples when narrow absorptions are targeted. However, the presented scripts are designed to show the concept rather than to provide the ultimate version of a feature extraction script. Table 9 lists the 16 feature extraction scripts next to the REEs that can be mapped by the respective script.

Table 9 Feature extraction scripts for VNIR-active REEs and REE absorption bands described by (Turner et al., 2016, 2014) and this work (d – doublet, m – medium, mb – medium & broad, s – strong, sh – shoulder, w – weak, weak & broad)

Feature extraction scripts			carbonates (Turner et al., 2016)							phosphates													
										monazite				xenotime				fluorapatite		apatite	
relative depth	wave-length position	radius	REE	bastnaesite		parisite		synchisite		Turner et al. (2014)		this work		Turner et al. (2014)		this work		Turner et al. (2014)		this work	
580D	580W	20	Nd	580	s	580	s	580	s	Nd	581	580	s					Nd	576	578	s
																		Nd	585	583	s
744D	744W	20								not assigned		737	s					Nd	738	738	m
			Nd	741	s	741	s	740	s	Nd	745	745	s	Dy>Ho, Nd?	740	740	w				
														Dy>Ho, Nd?	748	748	w	Nd	749	749	s
														Dy>Ho, Nd?	754	753	m				
														Dy>Ho, Nd?	760	761	m	Nd	763		
801D	801W	20	Nd	792	d	792	d	792	d			794	s	Dy>Er, Nd?	803			Nd	800		
			Nd	797	d	798	d	799	d	Nd	800	802	s	Dy>Er, Nd?	811			Nd	805	803	s
870D	870W	30	Nd	864	s	864	s	864	s	Nd	863	862	s	Nd	872	872	w	Nd	870	870	wb
			Nd	889		889		889		Nd	871	872	s								
										not assigned		886	m								
										not assigned		897	sh								
978D	978W	30	Sm	953		953		953	w	Sm	957	956	m	Dy, Yb, Sm	953	953	w				
														Yb, Er	977	977	m				
										Yb>Er	980			Yb, Er	978						
1091D	1091W	30								Sm	1074	1078	s								
			Sm	1093	s	1093		1093						Dy	1099	1099	mb				
										Sm	1105	1107	m			1115	mb				
1550D	1550W	30	Pr^{3+}>Sm^{3+}	1547	s	1547		1547	s	Sm?	1553	1549	mb	Er>Sm	1528	1538	mb				
			Pr^{3+}>Sm^{3+}>Nd^{3+}	1578		1578	sh	1578	sh							1561	sh			1547	wb
										not assigned		1584	mb			1588	mb			1579	wb
1700D	1700W	25								Dy, Nd	1691	1690	w	Dy	1704	1705	s				
			Nd	1710		1710		1710		Nd	1710	1716	w								
														Dy, Tb	1723	1726	m				

Based on the feature extraction scripts, Nd-related features at around 580, 740, 801 and 870 nm are strongest in monazite and parasite reference samples and less strong in apatite, bastnaesite and britholite (Figure 24a, b, c, d). Nd also appears to be present in eudialyte, although it doesn't show a strong 870 nm absorption (Figure 24d). In phosphates, a strong absorption feature in the 1700 nm wavelength range is either related to Nd, Dy or Tb (Turner et al., 2014). Amongst the reference samples, monazite shows a strong doublet in this wavelength region with its deepest feature being located either at 1694 or 1715 nm (Figure 24e).

Xenotime reference samples are characterised by a strong absorption feature at around 978 nm (Figure 25b), which can be attributed to either Yb or Er (Turner et al., 2014). Amongst the other presumably REE-bearing reference samples, only eudialyte shows an absorption feature in the same wavelength range (973 nm).

Monazite reference samples show a strong absorption at around 1080 nm, which can be assigned to Sm (Turner et al., 2014) and can be identified using the 1091D script (Figure 25c).

A range of REE elements such as Pr and Sm produce several absorptions in the 1550 nm wavelength range. The 1550D and 1550W scripts can be used to identify REEs in parasite confirming earlier published REE absorptions features in carbonates (Turner et al., 2016) and monazite (Turner et al., 2014). Eudialyte also shows an absorption at around 1538 nm. Furthermore, the 1550D and 1550W scripts highlight xenotime. However, the discussed scripts are not designed to map the large xenotime feature in this wavelength range, identifying the long wavelength slope of a strong and broad feature that is centred at 1503 nm. Importantly, the 1550D and 1550W scripts are also tracking a major absorption diagnostic for epidote-series minerals. However, this absorption is not related to REEs, but represents an overtone of hydroxyl-related stretching fundamentals in epidote (Langer and Raith, 1974).

The feature extraction scripts presented here work well in pure / single mineral samples, but can also be applied in mixed mineral assemblages. For example, the 744D script was applied to map the relative abundance of Nd in drill core DD84CDD1 from the Cummins Range carbonatite in Western Australia (Huntington and Laukamp, 2015). However, many of the REE-focussed feature extraction scripts are heavily compromised when ferrous and/or ferric iron is present, such as in iron oxides or carbonates. The presence of iron must be taken into account when applying the feature extraction scripts, especially when sections with different relative amounts of ferrous and/or ferric iron are compared with each other.

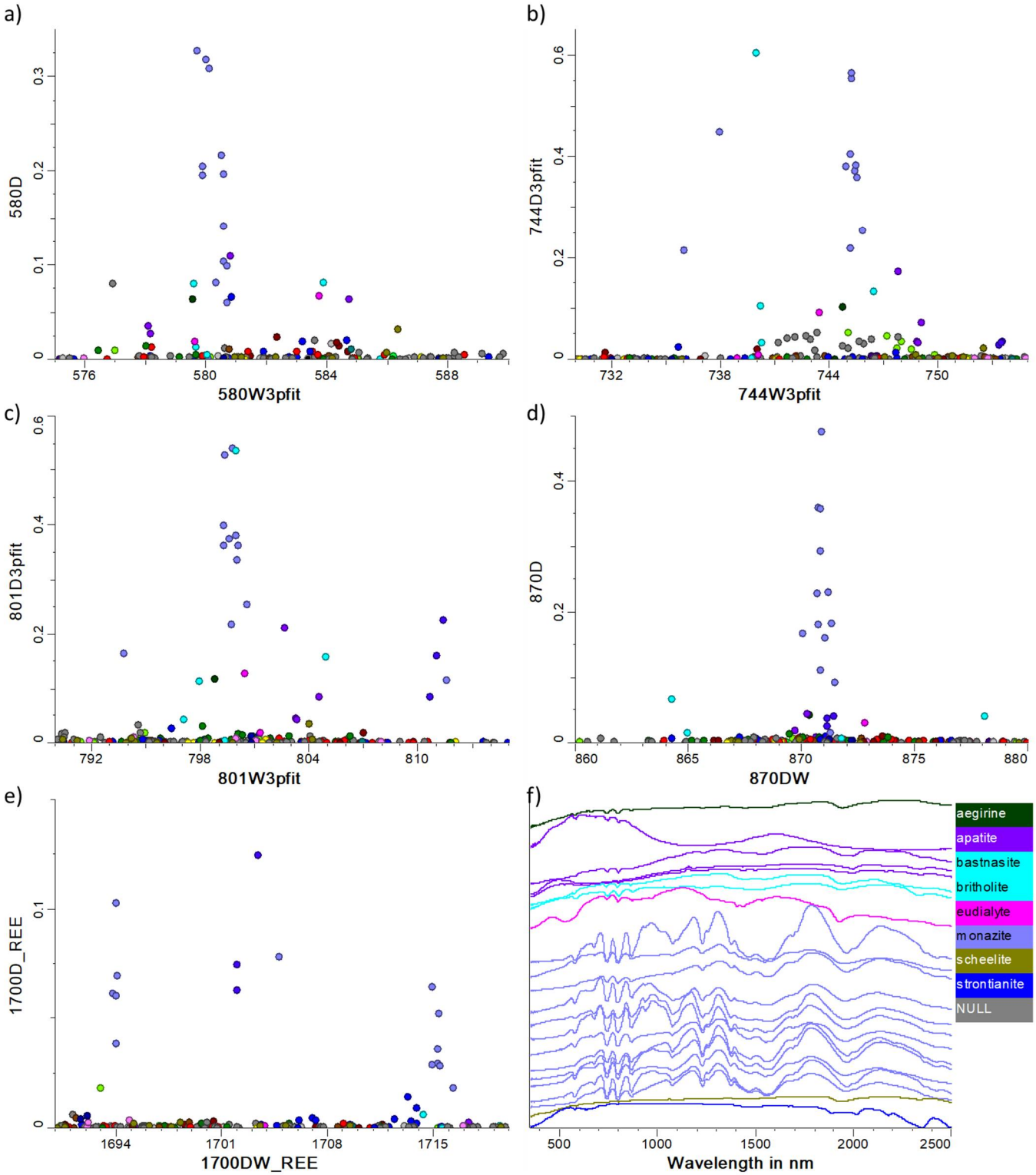

Figure 24 Wavelength position and relative intensity of (mainly) Nd-related absorption features determined by means of feature extraction scripts listed in Table 9. Reflectance spectra of reference samples with strong Nd-related absorptions are shown in f).

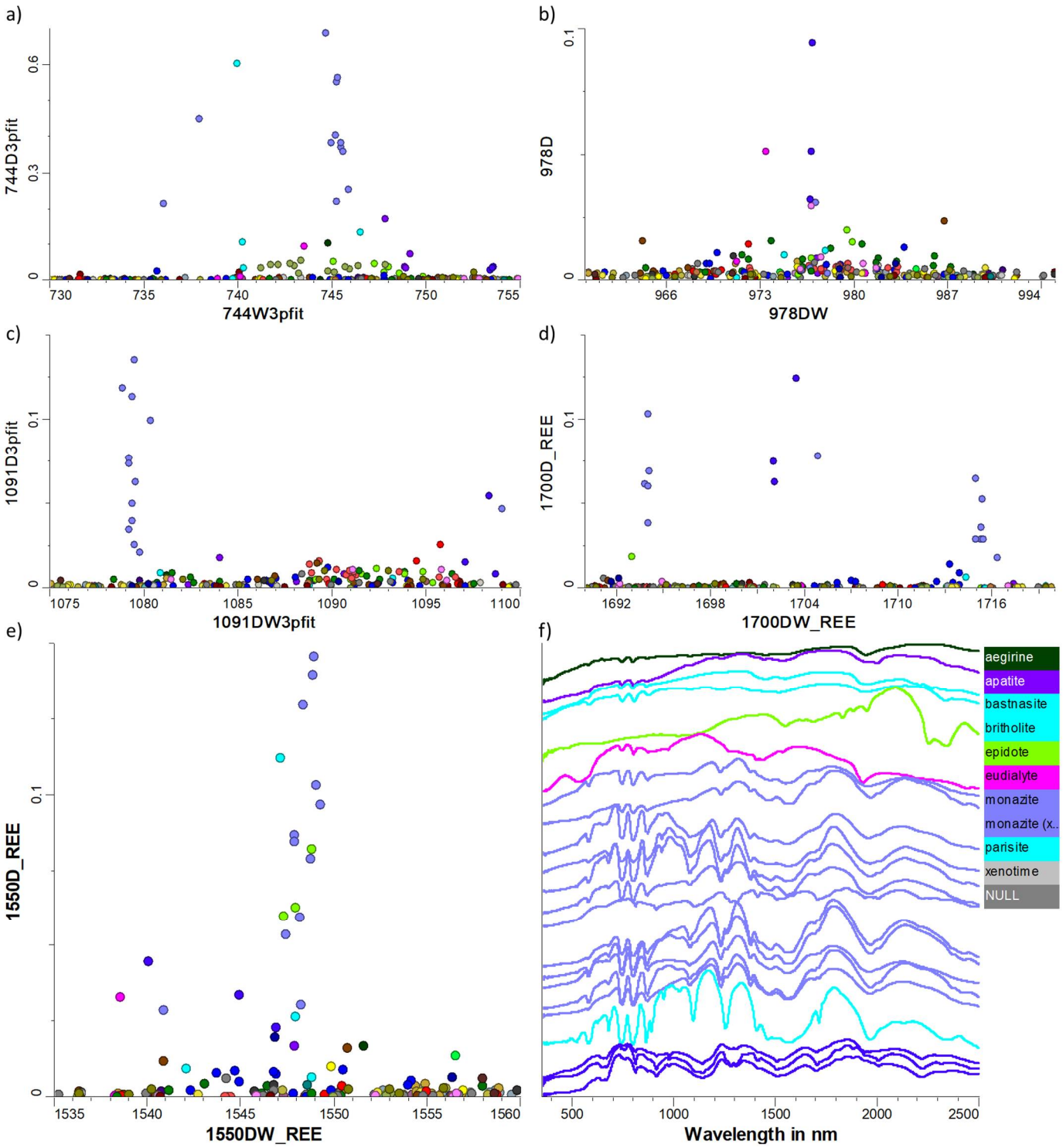

Figure 25 Wavelength position and relative intensity of (mainly) REE-related (other than Nd) absorption features determined by means of feature extraction scripts listed in Table 9. Reflectance spectra of reference samples with strong REE-related absorptions are shown in f).

6 Summary and recommendations

This report describes CSIRO's visible to near-infrared spectral reference library (VNIR SRL 2.0). For the VNIR SRL 2.0, about 2000 mineral sample candidates were assessed for their purity and usability in the spectral reference library according to 1) previous analytical data such as XRD, 2) examination of previous FTIR spectra over the entire MIR wavelength range and 3) visual inspection. Of the samples that were evaluated, only 279 mineral samples were deemed suitable for inclusion in the VNIR SRL 2.0. The VNIR SRL 2.0 comprises reflectance spectra of 279 mineral samples over the 350 to 2500 nm wavelength range, which were acquired from single crystals, crystal aggregates, sand, pulp and rocks. The VNIR and SWIR reflectance spectra were assessed for features pertaining to the respective minerals of interest along with impurities related to associated minerals and other contaminants. In some cases, independent validation data (e.g. X-ray diffraction, scanning electron microscopy, inductively coupled plasma spectrometry and Fourier transform infrared spectroscopy) were used to evaluate the purity of the reference sample candidates. The resulting VNIR SRL 2.0 collection comprises representatives from the following mineral groups: sulfides, oxides, hydroxides, carbonates, sulfates, phosphates, molybdates/tungstates, nesosilicates, cyclosilicates, inosilicates and phyllosilicates.

6.1 Recommendations

Presented here is just the second and updated version of the VNIR spectral reference library (VNIR SRL 2.0). The collection is not comprehensive in that it doesn't represent the full variability of VNIR spectral signatures of rock forming and key alteration minerals. The following steps are recommended for improving the VNIR spectral reference library (not in order of priority):

- Outstanding validation of selected samples and most of this is scheduled for FY23. Further geochemical and compositional analysis (e.g. ICP, QXRD, SEM, etc) is required on some of the mineral/rock samples prior to inclusion in the final reference library;
- Re-assessing the suitability of each VNIR SRL 2.0 sample for inclusion in the TSG library for mineral matching. TSA/TSG studies that use the reference spectra obtained in this report against known mineral mixtures would be valuable and a requirement of validation;
- The generation of a test dataset to enable an evaluation of the performance of TSAV;
- Scanning each reference sample using the HyLogger-4 (pending on arrival of HyLogger4 at GSWA's core library in Carlisle). This is needed to ensure that the reference spectra are relevant and that the spectral resolution/quality is comparable to real samples that will be measured in the future;
- Once validation and all spectral QA/QC has been achieved, then upload the reference VNIR spectra and metadata to CSIRO's online spectral library.

References

Adams, J.W., 1965. The visible region absorption spectra of rare-earth minerals1. Am. Mineral. 50, 356–366.

Berman, M., Bischoff, L., Lagerstrom, R., Guo, Y., Huntington, J., Mason, P., Green, A.A., 2017. A comparison between three sparse unmixing algorithms using a large library of shortwave infrared mineral spectra. IEEE Transactions on Geoscience and Remote Sensing 55, 3588–3610. https://doi.org/10.1109/TGRS.2017.2676816

Burns, R.G., 1993. Mineralogical Applications of Crystal Field Theory, 2nd ed. Cambridge University Press. https://doi.org/10.1017/CBO9780511524899

Cudahy, T.J., Ramanaidou, E.R., 1997. Measurement of the hematite:goethite ratio using field visible and near-infrared reflectance spectrometry in channel iron deposits, Western Australia. Aust. J. Earth Sci. 44, 411–420. https://doi.org/10.1080/08120099708728322

Fassel, V.A., 1961. Analytical spectroscopy of the rare-earth elements, in: The Rare Earths. John Wiley and Sons, New York, pp. 594–613.

Gaines, R.V., Dana, J.D. (Eds.), 1997. Dana's new mineralogy, 8., ed. entirely rewritten and greatly enl. ed. Wiley, New York, NY.

Huntington, J.F., Laukamp, C., 2015. Drill Core Reflectance Spectroscopy Applied to the Carbonatite Hosted REE Deposit at Cummins Range (Australia), in: Proceedings. Presented at the 13th SGA Biennial Meeting 2015, Dublin, Ireland.

Izawa, M.R.M., Cloutis, E.A., Rhind, T., Mertzman, S.A., Poitras, J., Applin, D.M., Mann, P., 2018. Spectral reflectance (0.35–2.5 μm) properties of garnets: Implications for remote sensing detection and characterization. Icarus 300, 392–410. https://doi.org/10.1016/j.icarus.2017.09.005

Langer, K., Raith, M., 1974. Infrared spectra of Al-Fe(III)-epidotes and zoisites, Ca2(Al1-p Fe3+p)Al2O(OH)[Si2O7][SiO4]. Am. Mineral. 59, 1249–1258.

Laukamp, C., Lau, I.C., Mason, P., Warren, P., Huntington, J.F., Green, A.A., Whitbourn, L., Wright, W., Connor, P., 2015a. CSIRO Thermal infrared spectral library – Part 1: Evaluation and status report 2015 (No. EP155769).

Laukamp, C., McFarlane, A.J., Montenegro, V., Voisin, L., Palma, G., 2015b. Rapid Resource Characterisation of Cu-Chlorides and Sulphates in Porphyry Cu Deposits using Reflectance Spectroscopy, in: Proceedings. Presented at the 13th SGA Biennial Meeting 2015.

LeGras, M., Lau, I.C., 2019. NVCL Spectral Reference Library - Scapolites (No. EP193519).

LeGras, M., Laukamp, C., 2019. NVCL Spectral Reference Library - Pyroxenes and Pyroxenoids (CSIRO Report No. EP184276). CSIRO.

LeGras, M., Laukamp, C., Lau, I., Mason, P., 2018. NVCL Spectral Reference Library - Phyllosilicates Part 2: Micas (CSIRO Report No. EP183095). CSIRO.

LeGras, M., Laukamp, C., Lau, I.C., Mason, P., 2019. NVCL Spectral Reference Library - Al2SiO5 Polymorphs (No. EP197601).

Lorenz, S., Beyer, J., Fuchs, M., Seidel, P., Turner, D., Heitmann, J., Gloaguen, R., 2018. The Potential of Reflectance and Laser Induced Luminescence Spectroscopy for Near-Field Rare Earth Element Detection in Mineral Exploration. Remote Sens. 11, 21. https://doi.org/10.3390/rs11010021

Morin Ka, S., 2011. Hyperspectral characterisation of rare-earth elements. Curtin University.

Pejcic, B., Shelton, T., LeGras, M., Laukamp, C., Francis, N., Lau, I.C., 2021. Mid infrared spectral library (No. EP2021-1148).

Rowan, L.C., Kingston, M.J., Crowley, J.K., 1986. Spectral reflectance of carbonatites and related alkalic igneous rocks; selected samples from four North American localities. Econ. Geol. 81, 857–871. https://doi.org/10.2113/gsecongeo.81.4.857

Schodlok, M.C., Green, A., Huntington, J., 2016a. A reference library of thermal infrared mineral reflectance spectra for the HyLogger-3 drill core logging system. Aust. J. Earth Sci. 63, 941–949. https://doi.org/10.1080/08120099.2016.1234508

Schodlok, M.C., Whitbourn, L., Huntington, J., Mason, P., Green, A., Berman, M., Coward, D., Connor, P., Wright, W., Jolivet, M., Martinez, R., 2016b. HyLogger-3, a visible to shortwave and thermal infrared reflectance spectrometer system for drill core logging: functional description. Aust. J. Earth Sci. 63, 929–940. https://doi.org/10.1080/08120099.2016.1231133

Turner, D.J., Rivard, B., Groat, L.A., 2018. Visible and short-wave infrared reflectance spectroscopy of selected REE-bearing silicate minerals. Am. Mineral. 103, 927–943. https://doi.org/10.2138/am-2018-6195

Turner, D.J., Rivard, B., Groat, L.A., 2016. Visible and short-wave infrared reflectance spectroscopy of REE phosphate minerals. Am. Mineral. 101, 2264–2278. https://doi.org/10.2138/am-2016-5692

Turner, D.J., Rivard, B., Groat, L.A., 2014. Visible and short-wave infrared reflectance spectroscopy of REE fluorocarbonates. Am. Mineral. 99, 1335–1346. https://doi.org/10.2138/am.2014.4674

White, W.B., 1967. Diffuse-Reflectance Spectra of Rare-Earth Oxides. Appl. Spectrosc. 21, 167–171. https://doi.org/10.1366/000370267774385173

Wood, B.J., Strens, R.G.J., 1979. Diffuse reflectance spectra and optical properties of some sulphides and related minerals. Mineral. Mag. 43, 509–518. https://doi.org/10.1180/minmag.1979.043.328.11

Appendix A VNIR SRL version 2.0 – list of reference samples

This table provides details about the type, locality, available additional analytical results and references for each of the reference samples.

- Column A: "VNIR Index" – is available in tsg files "VNIR_SRL_2pt0.tsg" and can be used to import additional data from "VNIR_SRL_report_AppendixA.xlsx" into TSG-file
- Column B: "Sample name"
- Column C: "accepted VNIR reflectance spectrum for report" – FieldSpec3 reflectance spectrum that was chosen for the final VNIR SRL 2.0
- Column D: "MIR SRL 1.0 (Pejcic et al., 2021)" – highlights if sample is present in MIR SRL 1.0
- Column E: "to do" – refers to next step with regards to validation and publishing
- Column F: "sample type" –
    - Single crystals: this includes crystals of various size, typically between 0.5 and 5 cm in length. Some single crystals contain visual impurities (e.g. white mica along spodumene cleavage), in which case the least impure side of the crystal was scanned with the FTIR.
    - Crystal aggregates: this includes aggregates of smaller crystals, typically between 0.05 and 0.5 cm in diameter, that are orientated in different ways to each other (e.g. randomly or radially). Crystal aggregates can include visibly small amounts of impurities.
    - Rock samples: these include all samples, where the target mineral is present in a mixed mineral assemblage and finely intergrown with other minerals, mostly at microscopic scale.
    - Pulp samples
- Column G: "detailed sample type" – more detailed description of sample type
- Column H: "2nd sample name" – sample names / numbers in addition to primary sample name listed in column B
- Column I: "Reference" – Literature reference if available. Otherwise collection.
- Column J: "Location" – locality/source of sample
- Column K: "physical location of sample" – referring either to collection (e.g. Mitchell Collection) or drawer in NVCL collection. For example, ARRC2D06A3 is located at "ARRC" = Building (Australian Resources Research Centre, Kensington, 6151 WA); 2D06 = room number in ARRC building; "A3" = sample cabinet "A", third drawer/section from top. The

number/letter code can also be found on a label of the respective drawer. A full list of samples in ARRC2D06 is available from the NVCL project team on request.

- Column L: chapter in report
- Columns M/N/O: Main mineral species / group of interest and respective general chemical formula (according to IMA)
- Column P: Mineral group classification in preparation for potential development of mineral matching algorithm (for pure and 80% pure samples only)
- Columns Q: XRD/geochemistry-based mineral assemblage
- Column R: XRD mineral group class of targeted mineral
- Column S: Purity of reference mineral, classified according to:
    - "Pure (GT90 XRD)": target mineral species amounts to +90% according to XRD
    - "80% pure (90to80)": target mineral species amounts to 80 to 90% according to XRD
    - "Impure (LT80)": target mineral species amounts to less than 80% according to XRD.
- Column T: Impurities (based on XRD)/ (based on chemistry)
- Columns U to HA: available XRD results and references
- Columns HB to JM: available whole rock geochemistry
- Columns JN to KA: available SEM results and references
- Columns KB to KV: available EPMA results and references
- Columns KW to MA: available XRF results and references

Appendix B Mineral group and species classification according to Dana (Gaines and Dana, 1997)

	Dana class	Dana class Nr	Dana group/subgroup	Dana group/ subgroup Nr	Dana mineral	Dana mineral Nr	MIR SRL group	MIR SRL subgroup	Nr of spectra in draft VNIR SRL 2.0
Native Elements	Native Elements - with metallic elements other than the platinum group	1.01	Gold Group	01.01.01.	gold	01.01.01.01	native elements	native elements	1
					copper	01.01.01.03			3
	Native Elements - with semi-metallic and non-metallic elements	1.03	Sulfur Polymorph group		sulphur	01.01.05.01			2
Sulfide Minerals	Sufides - including Selenides and Tellurides where Am Bn Xp, with (m+n):p=2:1	2.04	Chalcocite Group	02.04.01	chalcocite	02.04.02.01	sulfide group	sulfide group	13
			Stromeyerite Group	02.04.06	stromeyerite	02.04.06.01			1
	Sufides - including Selenides and Tellurides where Am Bn Xp, with (m+n):p=3:2	2.05	n.a.	02.05.02	bornite	02.05.02.01			13
	Sufides - including Selenides and Tellurides where Am Bn Xp, with (m+n):p=1:1	2.08	Galena Group	02.08.01	galena	02.08.01.01			4
			Sphalerite Group	02.08.02	sphalerite	02.08.02.01			2
			n.a.	02.08.10	pyrrhotite	02.08.10.01			2
			Nickeline Group	02.08.11	nickeline	02.08.11.01			2
			Covellite Group	02.08.12	covellite	02.08.12.01			3
			Cobaltite Group	02.08.13	cobaltite	02.08.13.01			1
			n.a.	02.08.14	cinnabar	02.08.14.01			2
	Sufides - including Selenides and Tellurides where Am Bn Xp, with (m+n):p=1:1	2.09	Chalcopyrite Group	02.09.01	chalcopyrite	02.09.01.01			15
			Stannite Group	02.09.02	stannite	02.09.02.01			1
	Sufides - including Selenides and Tellurides where Am Bn Xp, with (m+n):p=2:3	2.11	Stibnite Group	02.11.02	stibnite	02.11.02.01			13
	Sufides - including Selenides and Tellurides where Am Bn Xp, with (m+n):p=1:2	2.12	Pyrite Group	02.12.01	pyrite	02.12.01.01			9
			Marcasite Group	02.12.02	marcasite	02.12.02.01			1
					lollingite	02.12.02.09			1
			Arsenopyrite Group	02.12.04	arsenopyrite	02.12.04.01			8
			Molybdenite Group	02.12.10	molybdenite	02.12.10.01			7
	Sulfides - where 3 < z/y < 4 - (A+)i (A++)j [By Cz], A=metals, B=semi-metals, C=non-metals	3.03	Tetrahedrite Group	03.03.06	tetrahedrite	03.03.06.01			2
					tennantite	03.03.06.02			1
	Sulfides - where z/y > 3 - (A+)i (A++)j [By Cz], A=metals, B=semi-metals, C=non-metals	3.04	Proustite Group	03.04.01	proustite	03.04.01.01			1
					pyrargyrite	03.04.01.02			1
			n.a.	03.04.03	bournonite	03.04.03.02			2
	Sulfides - where 2.5 < z/y < 3 - (A+)i (A++)j [By Cz], A=metals, B=semi-metals, C=non-metals	3.05	n.a.	03.05.02	boulangerite	03.05.02.01			2
simple oxides	Simple Oxides with a cation charge of 1+ (A+2 O)	4.01	n.a.	04.01.01	cuprite	04.01.01.01			3
	Simple Oxides with a cation charge of 3+ (A+++2 O3)	4.03	Corundum-Hematite group (Rhombohedral: R-3c)	04.03.01	hematite	04.03.01.02	iron oxide tot	iron oxide tot	7
	Simple Oxides with a cation charge of 4+ (A++++ O2)	4.04	rutile group	04.04.01	cassiterite	04.04.01.05	rutile group	rutile group	1
Hydroxides and Oxides with OH	Hydroxides and Oxides Containing Hydroxyl where X+++O OH	6.01	Diaspore group (Orthorhombic, Pnma or Pnmd)	06.01.01	goethite	06.01.01.02	iron oxide tot	iron oxide tot	15
			Boehmite Group	06.01.02	lepidochrocite	06.01.02.02	iron oxide tot	iron oxide tot	1
multiple oxides	Multiple Oxides (A+ B++)2 X4 Spinel group	7.02	(Iron subgroup)	07.02.02	magnetite	07.02.02.03	iron oxide tot	iron oxide tot	3
hydroxyhalides	Oxyhalides and Hydroxyhalides where (A)2 (O,OH)3 Xq	10.01	Atacamite group	10.01.01	atacamite	10.01.01.01	Atacamite group	Atacamite group	2
carbonate	Anhydrous Carbonates with Simple Formula A+ CO3	14.01	Aragonite Group (Orthorhombic: Pmcn)	14.01.03	aragonite	14.01.03.01	carbonate group	carbonate group	1
					witherite	14.01.03.02			2
					strontianite	14.01.03.03			2
					cerussite	14.01.03.04			1
			Calcite Group (Trigonal: R-3c)	14.01.01	calcite	14.01.01.01			2
					magnesite	14.01.01.02			1
					siderite	14.01.01.03			2
					rhodochrosite	14.01.01.04			3
					gaspeite	14.01.01.08			3
	Anhydrous Carbonates with Compound Formula A+ B++ (CO3)2	14.02	Dolomite Group (Trigonal: R-3)	14.02.01	dolomite	14.02.01.01			4
					ankerite	14.02.01.02			1
	Carbonates - Hydroxyl or Halogen in the Bastnasite/Shynchysite/ Parasite Groups	16a.01	Bastnasite Group	16a.01.01	bastnasite	n.a.			1
					bastnasite-(Y)	16a.01.01.03			1
			Synchysite Group	16a.01.03	synchysite-(Ce)	16a.01.03.01			1
			Parisite Group	16a.01.05	parisite	16a.01.05.02			1
	Carbonates - Hydroxyl or Halogen where (A B)3 (XO3)2 Zq	16a.02	NULL	16a.02.01	azurite	16a.02.01.01			5
	Carbonates - Hydroxyl or Halogen where (A B)2 (XO3) Zq	16a.03	Malachite Group	16a.03.02	malachite	16a.03.02.01			5
			Sjorgrenite-Hydrotalcite Group (Sojogrenite Subgroup:Rhombohedral)	16b.06.02	pyroaurite	16b.06.02.03			1
Anhydrous Sulfates with OH or Halogen	Anhydrous Sulfates Containing Hydroxyl or Halogen where (A B)m (XO4)p Zq where m:p>2:1	30.01	NULL	30.01.12	antlerite	30.01.12.01	sulfate group	sulfate group	0
	Anhydrous Sulfates Containing Hydroxyl or Halogen where (A B)2 XO4 Zq	30.02	Alunite Group (Jarosite Subgroup)	30.02.05	jarosite	30.02.05.01			2

	Dana class	Dana class Nr	Dana group/subgroup	Dana group/ subgroup Nr	Dana mineral	Dana mineral Nr	MIR SRL group	MIR SRL subgroup	Nr of spectra in draft VNIR SRL 2.0
anhydrous phosphates	anhydrous phosphates, etc	38.04	Monazite Group	38.04.03	monazite	n.a.	phosphate group	monazite group	13
					monazite-(Ce)	38.04.03.01			
					monazite-(La)	38.04.03.02			
					monazite-(Nd)	38.04.03.05			
					monazite-(Sm)	38.04.03.07			
			Xenotime Group	38.04.11	Xenotime	n.a.		Xenotime Group	3
					Xenotime-(Y)	38.04.11.01			
	anhydrous phosphates where (A)5 (XO4)3 Zq	41.08	Apatite Group	41.08.01	apatite	41.08.01.00		apatite group	4
	anhydrous phosphates where (A)5 (XO4)3 Zq	41.08	Apatite Group	41.08.01	apatite-(CaF)	41.08.01.01			0
Anhydrous Molybdates and Tungstates	Anhydrous Molybdates and Tungstates where A XO4	48.01	Wolframite Series	48.01.01	wolframite	48.01.01.00	wolframite series	wolframite series	9
			Scheelite Series	48.01.02	scheelite	48.01.02.01	scheelite series	scheelite series	2
nesosilicate	Nesosilicate Insular SiO4 Groups Only with cations in [4] coordination	51.01	Phenakite group	51.01.01	willemite	51.01.01.02	Phenakite group	Phenakite group	1
	Insular SiO4 Groups Only	51.03	Olivine group	51.03.01	olivine	tbd	olivine group	olivine group	2
					fayalite	51.03.01.01			1
					forsterite	51.03.01.02			2
	Nesosilicate Insular SiO4 Groups Only with cations in [6] and >[6] coordination	51.04	Garnet group (Pyralspite series)	51.04.03a	pryralspite	tbd	garnet group	pyralspite series	2
					pyrope	51.04.03a.01			2
					almandine	51.04.03a.02			2
					spessartine	51.04.03a.03			1
					calderite	51.04.03a.06			1
			Garnet group (Ugrandite series)	51.04.03b	andradite	51.04.03b.01		ugrandite series	2
					grossular	51.04.03b.02			1
					uvarovite	51.04.03b.03			3
	Nesosilicate Insular SiO4 Groups and O, OH, F, and H2O with cations in [6] and >[6] coordination	52.04	Silicate apatites	52.04.09	britholite	52.04.09.01	Silicate apatites	Silicate apatites	2
sorosilicate	Sorosilicates Sorosilicate Insular, Mixed, Single, and Larger Tetrahedral Groups with cations in [6] and higher coordination; single and double groups (n=1,2)	58.02	Epidote group (Clinozoisite subgroup)	58.02.01a	epidote	58.02.01a.02	epidote group	epidote group	3
cyclosilicate	Cyclosilicates Cyclosilicate Six-Membered Rings with borate groups	61.03	n.a.	n.a.	tourmaline	n.a.	tourmaline group	tourmaline group	5
			Elbaite Subgroup	61.03d.01	elbaite	61.03d.01.08			
			Schorl Subgroup	61.03e.01	dravite	61.03e.01.09			
					schorl	61.03e.01.10			
	Cyclosilicate Rings with Other Anions and Insular Silicate Groups with mixed ring types	64.01	eudialyte group	64.01.01	eudialyte	64.01.01.01	eudialyte group	eudialyte group	3
inosilicate	Inosilicates Single-Width Unbranched Chains, W=1 with chains P=2	65.01	C2/c clinopyroxenes (Ca clinopyroxenes)	65.01.03a	augite	65.01.03a.03	pyroxene	clinopyroxene	3
				65.01.03a	diopside	65.01.03a.01			3
				65.01.03a	hedenbergite	65.01.03a.02			3
			C2/c clinopyroxenes (intermediate clinopyroxenes)	65.01.03b	omphacite	65.01.03b.01			0
			C2/c clinopyroxenes (Na clinopyroxenes)	65.01.03c	aegirine	65.01.03c.02			1
			P2/c clinopyroxenes	65.01.01	pigeonite	65.01.01.04			0
			orthopyroxenes	65.01.02	enstatite	65.01.02.01		orthopyroxene	3
			orthopyroxenes	65.01.02	ferrosilite	65.01.02.02			0
	Inosilicates Single-Width Unbranched Chains, W=1 with chains P=5	65.04	Rhodonite group	65.04.01	rhodonite	65.04.01.01	pyroxenoid	pyroxenoid	3
	Inosilicates Single-Width Unbranched Chains, W=1 with chains P=7	65.06	Pyroxmangite group	65.06.01	pyroxmangite	65.06.01.01	pyroxmangite	pyroxmangite	1
	Inosilicates Double-Width Unbranched Chains, W=2 with P=2	66.01	NULL	NULL	amphibole unclassified	NULL	amphibole	other amphibole	0
			Group 2, the calcic amphiboles	66.01.03a	actinolite	66.01.03a.01		calcic amphibole	2
	Inosilicate Chains with Side Branches or Loops, with P>2	69.02	Aenigmatite and related species (Aenigmatite subgroup)	69.02.01a	rhonite	69.02.01a.05	other inosilicate	rhonite	1
phyllosilicate	Phyllosilicates Phyllosilicate Sheets of Six-Membered Rings with 2:1 Layers	71.02	biotite subgroup ("dark mica")	71.02.02b	biotite	71.02.02b.02	micas	biotite subgroup ("dark mica")	5
					phlogopite	71.02.02b.01			1
			muscovite subgroup ("white mica")	71.02.02a	muscovite	71.02.02a.01		muscovite subgroup ("white mica")	0
					fuchsite	NULL			1
	Phyllosilicates Phyllosilicate Modulated Layers with joined strips	74.03	Palygorskite-sepiolite group (Sepiolite subgroup)	74.03.01b	falcondoite (garnierite)	74.03.01b.02	palygorskite-sepiolite group	palygorskite-sepiolite group	2
		74.03	NULL	74.03.02	chrysocolla	74.03.02.01	chrysocolla	chrysocolla	5

Appendix C TSG files

- The reflectance spectra were imported into the TSG file “VNIR_SRL_2pt0.tsg”. The TSG file is available from the NVCL project team on request.

Appendix D Sample pictures

The sample pictures are stored at CSIRO. A full list of samples in ARRC2D06 is available from the NVCL project team on request.

As Australia's national science agency and innovation catalyst, CSIRO is solving the greatest challenges through innovative science and technology.

CSIRO. Unlocking a better future for everyone.

Contact us

1300 363 400
+61 3 9545 2176
csiroenquiries@csiro.au
csiro.au

For further information

C**SIRO Mineral Resources**
Carsten Laukamp
+61 8 6436 8754
Carsten.Laukamp@csiro.au
https://www.auscope.org.au/nvcl

C**SIRO Mineral Resources**
Bobby Pejcic
+61 8 6436 8814
Bobby.Pejcic@csiro.au